

# Mutual Information-Maximizing Quantized Belief Propagation Decoding of Regular LDPC Codes

Xuan He<sup>†</sup>, Kui Cai<sup>‡</sup>, Zhen Mei<sup>\*</sup>, Peng Kang<sup>‡</sup>, and Xiaohu Tang<sup>†</sup>

<sup>†</sup>Southwest Jiaotong University, Chengdu 611756, China

<sup>‡</sup>Singapore University of Technology and Design, Singapore 487372, Singapore

<sup>\*</sup>Nanjing University of Science and Technology, Nanjing 210094, China

Email: xhe@swjtu.edu.cn, cai\_kui@sutd.edu.sg, meizhen@njjust.edu.cn, peng\_kang@sutd.edu.sg, xhutang@swjtu.edu.cn

**Abstract**—In this paper, we propose a class of finite alphabet iterative decoder (FAID), called mutual information-maximizing quantized belief propagation (MIM-QBP) decoder, for decoding regular low-density parity-check (LDPC) codes. Our decoder follows the reconstruction-calculation-quantization (RCQ) decoding architecture that is widely used in FAIDs. We present the first complete and systematic design framework for the RCQ parameters, and prove that our design with sufficient precision at node update is able to maximize the mutual information between coded bits and exchanged messages. Simulation results show that the MIM-QBP decoder can always considerably outperform the state-of-the-art mutual information-maximizing FAIDs that adopt two-input single-output lookup tables for decoding. Furthermore, with only 3 bits being used for each exchanged message, the MIM-QBP decoder can outperform the floating-point belief propagation decoder at the high signal-to-noise ratio regions when testing on high-rate LDPC codes with a maximum of 10 and 30 iterations.

**Index Terms**—Finite alphabet iterative decoder (FAID), lookup table (LUT), low-density parity-check (LDPC) code, mutual information (MI), quantized belief propagation (QBP).

## I. INTRODUCTION

Low-density parity-check (LDPC) codes [1] have been widely applied to communication and data storage systems due to their capacity approaching performance. Many of these systems, such as the NAND flash memory, have strict requirements on the memory consumption and implementation complexity of LDPC decoders [2], [3]. For the sake of simple hardware implementation, many efforts have been devoted to efficiently represent messages for LDPC decoding [4]–[11]. For example, in [4] and [5], the messages exchanged within the LDPC decoders are represented by log-likelihood ratios (LLRs) in low resolutions, which have generally 5 to 7 bits. The works in [6]–[11] develop the finite alphabet iterative decoder (FAID) for LDPC codes, which make use of messages represented by symbols from finite alphabets rather than by LLRs for decoding. These FAIDs draw much attention due to their excellent error rate performance and low decoding complexity. More specifically, they adopt the quantized messages of only 3 or 4 bits to approach and even surpass the performance of the floating-point belief propagation (BP) decoder [12]. In this paper, we focus on the class of FAIDs.

The early FAIDs investigated in [6]–[8] consider simple mappings, additions, and non-uniform quantization for decoding, leading to a reconstruction-calculation-quantization

(RCQ) decoding architecture. However, the design of these FAIDs (RCQ parameters) focuses on the specific class of (3, 6) (variable node (VN) degree 3 and check node (CN) degree 6) LDPC codes and requires large amount of manual optimizations. Thus, one can hardly generalize the decoder design to different scenarios. Recently, the mutual information-maximizing FAIDs (MIM-FAIDs) [9]–[11] are designed by density evolution (DE) [6] for various bit width settings of the decoder, with the aim of maximizing the mutual information (MI) between the coded bits and the exchanged messages within the decoder. These MIM-FAIDs are also referred to as MIM lookup table (MIM-LUT) decoders, since they adopt a series of cascaded two-input single-output LUTs for decoding. However, concatenating LUTs causes the degradation of both mutual information and error rate performance.

To overcome the drawbacks of the FAIDs in [6]–[11], we have presented a mutual information-maximizing quantized belief propagation (MIM-QBP) decoder in [13]. The MIM-QBP decoder adopts the RCQ decoding architecture at both the CN and VN update similarly to the FAIDs in [6]–[8]. The main contribution of [13] is to establish a high-level principle for designing good RCQ parameters, aiming at maximizing the MI between the coded bits and the exchanged messages, for decoding any regular LDPC codes. The principle has enabled the development of many follow-up MIM-FAIDs [14]–[19]. These MIM-FAIDs' VN update follows the RCQ decoding architecture where the RCQ parameters are designed based on the principle established in [13]; Their CN update employs the min operation (like the min-sum decoder [4]) to simplify the RCQ decoding architecture used in the CN update of the MIM-QBP decoder, at the cost of slightly degrading error rate performance.

This paper, as the extended version of [13], presents the first complete and systematic design framework for the RCQ parameters of the MIM-QBP decoder. More specifically, Section III of this paper includes the design principle originally proposed in [13] and gives more explanations. The most important extension over [13] is that, this paper contains a new section (Section IV) to illustrate the optimality of a class of reconstruction functions (RFs) which can make the corresponding MIM-QBP decoder maximize the MI between the coded bits and the exchanged messages; Meanwhile, it presents a near-optimal design of practical RFs based on

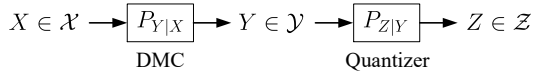


Fig. 1. Quantization of a discrete memoryless channel (DMC).

scaling the optimal RFs. Therefore, this paper essentially establishes a fundamental theory for supporting the validity of the aforementioned MIM-FAIDs [14]–[19]. Moreover, we believe that our design framework will facilitate the development of more follow-up MIM-FAIDs. The main contributions of this paper are summarized as follows:

- This paper presents, for the first time, a complete and systematic design framework of the RCQ parameters for decoding any regular LDPC codes.
- We prove that with sufficient precision for node update, our design for the RCQ parameters is able to maximize the MI between the coded bits and the exchanged messages.
- We investigate the error rate performance of the proposed MIM-QBP decoder based on extensive simulations. We observe that the MIM-QBP decoders can always considerably outperform the MIM-LUT decoders, and can sometimes even outperform the floating-point BP decoder with only 3 bits for each exchanged message.

The remainder of this paper is organized as follows. Section II first introduces the optimal quantization method for the binary-input discrete memoryless channel (DMC), and then gives a review of the MIM-LUT decoding and also highlights the linkage between the two topics. Section III illustrates the general design principle for designing the RCQ parameters for decoding regular LDPC codes. Section IV develops an efficient design of the RFs of the MIM-QBP decoder. Section V presents the simulation results. Finally, Section VI concludes this paper.

## II. PRELIMINARIES

### A. MIM Quantization of Binary-Input DMC

Due to the strong linkage between the MIM based channel quantization and the MIM based LDPC decoding message quantization, we first review the quantization of a binary-input DMC. As shown by Fig. 1, the channel input  $X$  takes values from  $\mathcal{X} = \{0, 1\}$  with probability  $P_X(0)$  and  $P_X(1)$ , respectively. The channel output  $Y$  takes values from  $\mathcal{Y} = \{y_1, y_2, \dots, y_N\}$  with channel transition probability given by  $P_{Y|X}(y_j|x) = Pr(Y = y_j|X = x)$ , where  $x = 0, 1$  and  $j = 1, 2, \dots, N$ . The channel output  $Y$  is quantized to  $Z$  which takes values from  $\mathcal{Z} = \{1, 2, \dots, M\}$ . A well-known criterion for channel quantization [20], [21] is to design a quantizer  $Q^* : \mathcal{Y} \rightarrow \mathcal{Z}$  to maximize the MI between  $X$  and  $Z$ , i.e.

$$\begin{aligned} Q^* &= \arg \max_Q I(X; Z) \\ &= \arg \max_Q \sum_{x \in \mathcal{X}, z \in \mathcal{Z}} P_{X,Z}(x, z) \log \frac{P_{X,Z}(x, z)}{P_X(x)P_Z(z)}, \quad (1) \end{aligned}$$

where  $P_{X,Z}(x, z) = P_X(x) \sum_{y \in \mathcal{Y}} P_{Y|X}(y|x)P_{Z|Y}(z|y)$  and  $P_Z(z) = \sum_{x \in \mathcal{X}} P_{X,Z}(x, z)$ .

A deterministic quantizer (DQ)  $Q : \mathcal{Y} \rightarrow \mathcal{Z}$  means that for each  $y \in \mathcal{Y}$ , there exists a unique  $z \in \mathcal{Z}$  such that  $P_{Z|Y}(z|y) = 1$  and  $P_{Z|Y}(z'|y) = 0$  for  $z \neq z' \in \mathcal{Z}$ . Let  $Q^{-1}(z) \subset \mathcal{Y}$  denote the preimage of  $z \in \mathcal{Z}$ . We name  $Q$  a sequential deterministic quantizer (SDQ) [21] if it can be equivalently described by an integer set  $\Lambda = \{\lambda_0, \lambda_1, \dots, \lambda_{M-1}, \lambda_M\}$  with  $\lambda_0 = 0 < \lambda_1 < \dots < \lambda_{M-1} < \lambda_M = N$  in the way given below

$$\begin{cases} Q^{-1}(1) = \{y_1, y_2, \dots, y_{\lambda_1}\}, \\ Q^{-1}(2) = \{y_{\lambda_1+1}, y_{\lambda_1+2}, \dots, y_{\lambda_2}\}, \\ \vdots \\ Q^{-1}(M) = \{y_{\lambda_{M-1}+1}, y_{\lambda_{M-1}+2}, \dots, y_{\lambda_M}\}. \end{cases}$$

We thus also name  $\Lambda$  an SDQ.

According to [20], there always at least exists a deterministic  $Q^*$  for (1) that can maximize  $I(X; Z)$ . Moreover,  $Q^*$  is an optimal SDQ if  $P_{Y|X}$  further satisfies

$$\frac{P_{Y|X}(y_1|0)}{P_{Y|X}(y_1|1)} \geq \frac{P_{Y|X}(y_2|0)}{P_{Y|X}(y_2|1)} \geq \dots \geq \frac{P_{Y|X}(y_N|0)}{P_{Y|X}(y_N|1)}, \quad (2)$$

where if  $P_{Y|X}(\cdot|1) = 0$ , we regard  $\frac{P_{Y|X}(\cdot|0)}{P_{Y|X}(\cdot|1)} = \infty$  as the largest value. (However,  $Q^*$  may not be an SDQ when (2) does not hold, in which case  $Q^*$  may not be simply described by the set  $\Lambda$ .) Note that after merging any two elements  $y, y' \in \mathcal{Y}$  with  $P_{Y|X}(y|0)/P_{Y|X}(y|1) = P_{Y|X}(y'|0)/P_{Y|X}(y'|1)$ , the resulting optimal quantizer is as optimal as the original one [20], [21]. A general framework has been developed in [21] for applying dynamic programming (DP) [22, Section 15.3] to find an optimal SDQ among all SDQs to maximize  $I(X; Z)$ . (The condition of (2) is not required, and if it holds, the optimal SDQ is an optimal DQ which can maximize  $I(X; Z)$  among all quantizers from  $\mathcal{Y}$  to  $\mathcal{Z}$ .)

### B. MIM-LUT Decoder Design for Regular LDPC Codes

Consider a binary-input DMC. Denote the channel input by  $X$  which takes values from  $\mathcal{X} = \{0, 1\}$  with equal probability, i.e.,  $P_X(0) = P_X(1) = 1/2$ . Denote  $L$  as the DMC output which takes values from  $\mathcal{L} = \{0, 1, \dots, |\mathcal{L}| - 1\}$  with channel transition probability  $P_{L|X}$ . Consider the design of a quantized message passing (MP) decoder for a regular  $(d_v, d_c)$  LDPC code, where  $d_v$  and  $d_c$  are the degrees of VNs and CNs, respectively. Denote  $\mathcal{R} = \{0, 1, \dots, |\mathcal{R}| - 1\}$  and  $\mathcal{S} = \{0, 1, \dots, |\mathcal{S}| - 1\}$  as the alphabets of variable-to-check (V2C) and check-to-variable (C2V) messages, respectively. Note that  $\mathcal{L}, \mathcal{R}, \mathcal{S}$  and their related functions may or may not vary with iterations. We use these notations without specifying the associated iterations since after specifying the decoder design for one iteration, the design is clear for all the other iterations.

For the V2C message  $R \in \mathcal{R}$  (resp. C2V message  $S \in \mathcal{S}$ ), we use  $P_{R|X}$  (resp.  $P_{S|X}$ ) to denote the probability mass function (pmf) of  $R$  (resp.  $S$ ) conditioned on the channel input bit  $X$ . If the code graph is cycle-free,  $R$  (resp.  $S$ )

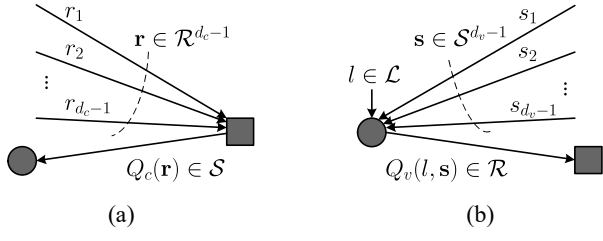


Fig. 2. Node update for mutual information-maximizing lookup table (MIM-LUT) decoding, where the circle and square represent a variable and check node, respectively. (a) Check node update. (b) Variable node update.

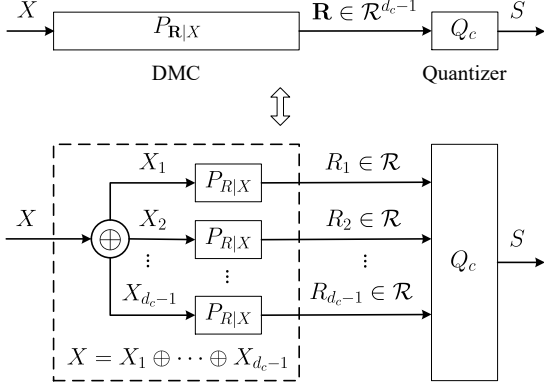


Fig. 3. Quantization of a discrete memoryless channel (DMC), where the quantizer works exactly the same as the check node update function  $Q_c$  for the mutual information-maximizing lookup table (MIM-LUT) decoding shown by Fig. 2(a).

conditioned on  $X$  is independent and identically distributed (i.i.d.) with respect to different edges for a given iteration. In the following, we introduce the design of the MIM-LUT decoder [9]–[11] based on density evolution (DE) [6]. In particular, DE is carried out to construct the LUTs of the message mappings for decoding by tracking the pmfs  $P_{R|X}$  and  $P_{S|X}$  at each iteration. Note that although a cycle-free code graph is assumed in the design of the MIM-LUT decoder, it still works well on code graphs containing cycles as shown in [9]–[11].

For each iteration, we first design the update function (UF)

$$Q_c : \mathcal{R}^{d_c-1} \rightarrow \mathcal{S} \quad (3)$$

for the CN update, which is shown by Fig. 2(a). The MIM-LUT decoding methods design  $Q_c$  to maximize  $I(X; S)$ . For easy understanding, we can equivalently convert it to the problem of DMC quantization, as shown by Fig. 3.

We assume  $P_{R|X}$  is known, since for the first iteration,  $P_{R|X}$  can be solely derived from the channel transition probability  $P_{L|X}$ , and for the other iteration,  $P_{R|X}$  is known after the design at VN is completed. The joint distribution  $P_{\mathbf{R}|X}$  of the incoming message  $\mathbf{R} \in \mathcal{R}^{d_c-1}$  conditioned on the channel input bit  $X$  (i.e., the channel transition probability  $P_{\mathbf{R}|X}$  of

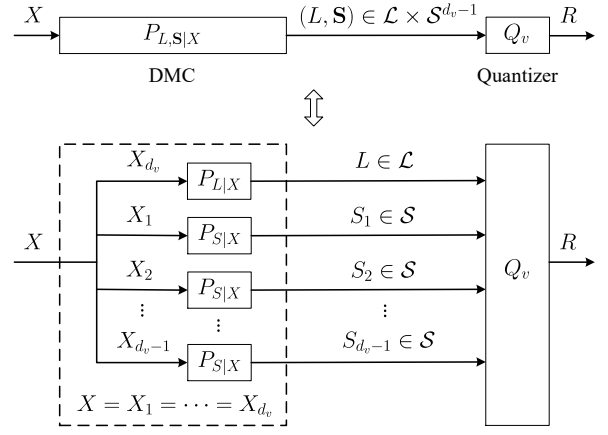


Fig. 4. Quantization of a discrete memoryless channel (DMC), where the quantizer works exactly the same as the variable node update function  $Q_v$  for the mutual information-maximizing lookup table (MIM-LUT) decoding shown by Fig. 2(b).

the DMC shown by Fig. 3) is given by [9]

$$P_{\mathbf{R}|X}(\mathbf{r}|x) = \left(\frac{1}{2}\right)^{\dim(\mathbf{r})-1} \sum_{\mathbf{x}:\oplus\mathbf{x}=x} \prod_{i=1}^{\dim(\mathbf{r})} P_{R_i|X}(r_i|x_i), \quad (4)$$

where  $\mathbf{r} = (r_1, r_2, \dots, r_{d_c-1}) \in \mathcal{R}^{d_c-1}$  is a realization of  $\mathbf{R}$ ,  $\dim(\mathbf{r}) = d_c - 1$  is the dimension of  $\mathbf{r}$ ,  $x \in \mathcal{X}$  is a realization of  $X$ ,  $\mathbf{x} = (x_1, x_2, \dots, x_{d_c-1}) \in \mathcal{X}^{d_c-1}$  consists of channel input bits corresponding to the VNs associated with incoming edges, and  $\oplus \mathbf{x} = x_1 \oplus x_2 \oplus \dots \oplus x_{d_c-1}$  with  $\oplus$  denoting the addition in  $GF(2)$ . Based on (4), we have

$$\begin{cases} P_{\mathbf{R}|X}(\mathbf{r}|0) \pm P_{\mathbf{R}|X}(\mathbf{r}|1) = \left(\frac{1}{2}\right)^{\dim(\mathbf{r})-1} \times \\ \quad \prod_{i=1}^{\dim(\mathbf{r})} (P_{R_i|X}(r_i|0) \pm P_{R_i|X}(r_i|1)), \\ P_{X|\mathbf{R}}(0|\mathbf{r}) \pm P_{X|\mathbf{R}}(1|\mathbf{r}) = \\ \quad \prod_{i=1}^{\dim(\mathbf{r})} (P_{X|R}(0|r_i) \pm P_{X|R}(1|r_i)). \end{cases} \quad (5)$$

Given  $P_{R|X}$ , the design of  $Q_c$  is equivalent to the design of  $Q^*$  in (1) by setting  $\mathcal{Y} = \mathcal{R}^{d_c-1}$  and  $\mathcal{Z} = \mathcal{S}$ . We can solve this design problem by using the DP method proposed in [20], after listing  $\mathbf{r}$  in descending order based on  $P_{\mathbf{R}|X}(\mathbf{r}|0)/P_{\mathbf{R}|X}(\mathbf{r}|1)$  (see (2)). After designing  $Q_c$ , the output message  $S$  is passed to the CN's neighbour VNs, with  $P_{S|X}$  being given by

$$P_{S|X}(s|x) = \sum_{\mathbf{r} \in Q_c^{-1}(s)} P_{\mathbf{R}|X}(\mathbf{r}|x). \quad (6)$$

We then proceed to design the UF

$$Q_v : \mathcal{L} \times \mathcal{S}^{d_v-1} \rightarrow \mathcal{R} \quad (7)$$

for the VN update, which is shown by Fig. 2(b). The MIM-LUT decoding methods also design  $Q_v$  to maximize  $I(X; R)$ . For easy understanding, we can equivalently convert it to the problem of DMC quantization, as shown by Fig. 4.

The joint distribution  $P_{L,S|X}$  of incoming message  $(L, \mathbf{S}) \in \mathcal{L} \times \mathcal{S}^{d_v-1}$  conditioned on the channel input bit  $X$  (i.e., the channel transition probability  $P_{L,S|X}$  of the DMC shown by

Fig. 4) is given by [9]

$$P_{L,S|X}(l, \mathbf{s}|x) = P_{L|X}(l|x) \prod_{i=1}^{\dim(\mathbf{s})} P_{S|X}(s_i|x), \quad (8)$$

where  $l \in \mathcal{L}$  is a realization of  $L$ ,  $\mathbf{s} = (s_1, s_2, \dots, s_{d_v-1}) \in \mathcal{S}^{d_v-1}$  is a realization of  $\mathbf{S}$ ,  $\dim(\mathbf{s}) = d_v - 1$  is the dimension of  $\mathbf{s}$ , and  $x \in \mathcal{X}$  is a realization of  $X$ .

Given  $P_{L,S|X}$ , the design of  $Q_v$  is equivalent to the design of  $Q^*$  in (1) by setting  $\mathcal{Y} = \mathcal{L} \times \mathcal{S}^{d_v-1}$  and  $\mathcal{Z} = \mathcal{R}$ . We can solve this design problem by using the DP method proposed in [20], after listing  $(l, \mathbf{s})$  in descending order based on  $P_{L,S|X}(l, \mathbf{s}|0)/P_{L,S|X}(l, \mathbf{s}|1)$  (see (2)). After designing  $Q_v$ , the output message  $R$  is passed to the VN's neighbour CNs, with  $P_{R|X}$  given by

$$P_{R|X}(r|x) = \sum_{(l, \mathbf{s}) \in Q_v^{-1}(r)} P_{L,S|X}(l, \mathbf{s}|x). \quad (9)$$

For each iteration, we can design the estimation function

$$Q_e : \mathcal{L} \times \mathcal{S}^{d_v} \rightarrow \mathcal{X} \quad (10)$$

to estimate the channel input bit corresponding to each VN. The design of  $Q_e$  can be carried out similarly to that of  $Q_v$ . The main differences involved in the design lie in the aspect that i) the incoming message alphabet  $\mathcal{L} \times \mathcal{S}^{d_v-1}$  is changed to  $\mathcal{L} \times \mathcal{S}^{d_v}$ ; and ii) the outgoing message alphabet  $\mathcal{R}$  is changed to  $\mathcal{X}$ . We thus ignore the details.

After completing the design of  $Q_c$ ,  $Q_v$ , and  $Q_e$  for all iterations, the design of the MIM-LUT decoder is completed. In general,  $|\mathcal{L}| = |\mathcal{R}| = |\mathcal{S}| = 8$  (resp. 16) is used for all iterations, leading to a 3-bit (resp. 4-bit) decoder. Given  $|\mathcal{L}|, |\mathcal{R}|, |\mathcal{S}|$ , and the maximum allowed decoding iterations  $I_{\max}$ , the design of the MIM-LUT decoder is determined by  $P_{L|X}$ . As shown in the literature [9]–[11],  $P_{L|X}$  depends on the choice of the noise standard derivation  $\sigma_d$  for designing the decoder parameters for an AWGN channel. We define the design threshold of an MIM-LUT decoder as

$$\sigma^* = \sup \left\{ \sigma_d : I^{(I_{\max})}(X; R) > 1 - \xi \right\}, \quad (11)$$

where  $I^{(I_{\max})}(X; R)$  is the value of  $I(X; R)$  computed after  $I_{\max}$  iterations, and  $\xi$  is a preset small number (e.g.  $10^{-2}$ ). Based on extensive simulations, by selecting  $\sigma_d = \sigma^*$ , the MIM-LUT decoder can achieve very good error rate performance across a wide range of signal-to-noise ratios (SNRs). However, the underlying reason remains an open problem.

Note that  $Q_c$ ,  $Q_v$ , and  $Q_e$  are stored as LUTs when implementing the MIM-LUT decoding. The sizes of the tables for  $Q_c$ ,  $Q_v$ , and  $Q_e$  are  $|\mathcal{R}|^{d_c-1}$ ,  $|\mathcal{L}| \cdot |\mathcal{S}|^{d_v-1}$ , and  $|\mathcal{L}| \cdot |\mathcal{S}|^{d_v}$ , respectively. Thus, a huge memory requirement may arise when the sizes of the tables are large in practice. To solve this problem, current MIM-LUT decoding methods [9]–[11] need to decompose  $Q_c$ ,  $Q_v$ , and  $Q_e$  into a series of two-input single-output LUTs. The decomposition can significantly reduce the cost of storage. However, it will degrade the performance of  $Q_c$ ,  $Q_v$ , and  $Q_e$  compared to the case without decomposition.

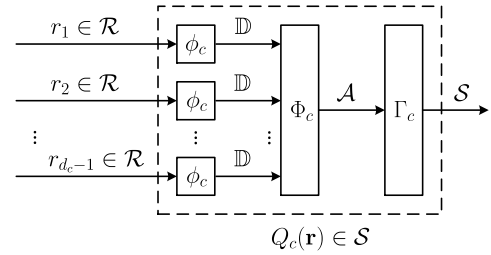


Fig. 5. Check node update for mutual information-maximizing quantized belief propagation (MIM-QBP) decoding. The part enclosed by the dash square corresponds to the update operation in the CN of Fig. 2(a).

### III. MIM-QBP DECODING FOR REGULAR LDPC CODES

In this section, we propose a general design framework for the MIM-QBP decoder. This decoder follows the RCQ decoding architecture and can be implemented based only on simple mappings and additions. Moreover, it can handle all incoming messages at a given node (CN or VN) simultaneously without causing any storage problem. As a result, the MIM-QBP decoder can greatly reduce the memory consumption and avoid the error rate performance loss due to table decomposition compared to the MIM-LUT decoder. In the following, we specify the design principles of the RCQ parameters at CN and VN, respectively.

#### A. CN Update for MIM-QBP Decoding

As shown by Fig. 5, the CN update for the MIM-QBP decoding proceeds the following three steps (reconstruction, calculation, and quantization): First, an RF  $\phi_c$  is used to map each V2C message symbol to a number of larger bit width which is called V2C computational message; second, we use a function  $\Phi_c$  to combine all V2C computational messages together as defined by (14) to form the C2V computational message; third, we use an SDQ  $\Gamma_c$  to quantize the C2V computational message into the C2V message symbol. In this way, the UF  $Q_c$  at the CN is fully determined by  $\phi_c$ ,  $\Phi_c$ , and  $\Gamma_c$ . In the rest of this subsection, we show the principles of designing  $\phi_c$ ,  $\Phi_c$ , and  $\Gamma_c$  so as to obtain a  $Q_c$  that can maximize  $I(X; S)$ .

1) *Design principle of  $\phi_c$* : We use an RF

$$\phi_c : \mathcal{R} \rightarrow \mathbb{D} \quad (12)$$

to map each V2C message realization  $r \in \mathcal{R}$  to a computational message  $\phi_c(r)$  in the computational domain  $\mathbb{D}$ , where we set  $\mathbb{D} = \mathbb{R}$  (real number set) or  $\mathbb{D} = \mathbb{Z}$  (integer set) for different considerations. Let  $\text{sgn}(\alpha)$  be the sign of  $\alpha \in \mathbb{R}$ , and

$$\text{sgn}(\alpha) = \begin{cases} -1 & \alpha < 0, \\ 0 & \alpha = 0, \\ 1 & \alpha > 0. \end{cases}$$

For  $r \in \mathcal{R}$ , let

$$LLR(r) = \log \left( P_{X|R}(0|r) / P_{X|R}(1|r) \right).$$

A good choice for  $\phi_c(r)$  based on empirical observation is

$$\begin{cases} \text{sgn}(\phi_c(r)) = \text{sgn}(\text{LLR}(r)), \\ |\phi_c(r)| \propto \frac{1}{|\text{LLR}(r)|}. \end{cases} \quad (13)$$

Based on (13), we associate  $\phi_c(r)$  to the channel input bit  $X$  in the following way: we predict  $X$  to be 0 if  $\text{sgn}(\phi_c(r)) > 0$  and to be 1 if  $\text{sgn}(\phi_c(r)) < 0$ , while  $|\phi_c(r)|$  indicates the *unreliability* of the prediction result (larger  $|\phi_c(r)|$  means less reliability). Note that the intuition behind (13) comes from [1] and [4]. In [1] and [4], the function  $f(\theta) = \log((e^\theta + 1)/(e^\theta - 1))$  is adopted by the CN update for any positive LLR value  $\theta$ , where  $f(\theta)$  decreases monotonically with  $\theta$ .

2) *Design principle of  $\Phi_c$* : For each V2C message realization  $\mathbf{r} \in \mathcal{R}^{d_c-1}$ , we combine all the V2C computational messages to form the C2V computational message as follows:

$$\Phi_c(\mathbf{r}) = \left( \prod_{i=1}^{\dim(\mathbf{r})} \text{sgn}(\phi_c(r_i)) \right) \sum_{i=1}^{\dim(\mathbf{r})} |\phi_c(r_i)|. \quad (14)$$

Similar to the CN update employed in [1] and [4], we predict  $X$  to be 0 if  $\text{sgn}(\Phi_c(\mathbf{r})) = \prod_{i=1}^{\dim(\mathbf{r})} \text{sgn}(\phi_c(r_i)) > 0$ , and to be 1 if  $\text{sgn}(\Phi_c(\mathbf{r})) < 0$ . Note that  $|\Phi_c(\mathbf{r})| = \sum_{i=1}^{\dim(\mathbf{r})} |\phi_c(r_i)|$  indicates the *unreliability* of the prediction result. Prediction in this way is consistent with the true situation shown by Fig. 3:  $X$  is the binary summation of the channel input bits associated with  $\mathbf{r}$ , which is determined by  $\text{sgn}(\phi_c(r_i))$ ,  $i = 1, 2, \dots, d_c - 1$ . More incoming messages lead to more unreliability (i.e., larger  $\dim(\mathbf{r})$  leads to larger  $|\Phi_c(\mathbf{r})|$ ). This is the reason why we use  $|\phi_c(r)|$  as the unreliability. The calculation step by (14) results in a set of distinct values of  $\Phi_c(\mathbf{r})$ ,  $\forall \mathbf{r} \in \mathcal{R}^{d_c-1}$ , which we denote by

$$\mathcal{A} = \{a_1, a_2, \dots, a_{|\mathcal{A}|}\}. \quad (15)$$

The elements in  $\mathcal{A}$  are labelled to satisfy

$$a_1 \succ a_2 \succ \dots \succ a_{|\mathcal{A}|}, \quad (16)$$

where  $\succ$  is a binary relation on  $\mathbb{R}$  defined by

$$\begin{aligned} \alpha \succ \beta &\iff \text{sgn}(\alpha) > \text{sgn}(\beta) \text{ or} \\ &(\text{sgn}(\alpha) = \text{sgn}(\beta) \text{ and } \alpha < \beta) \end{aligned}$$

for  $\alpha, \beta \in \mathbb{R}$ . For example, we have  $1 \succ 2 \succ 0 \succ -2 \succ -1$ . Assuming  $\Phi_c(\mathbf{r}) = a_i$ , we know from (16) that it is more likely to predict  $X$  to be 0 for smaller  $i$  and to be 1 for larger  $i$ . Thus, the listing order of (16) has a similar feature as that of (2). Let  $A$  be a random variable taking values from  $\mathcal{A}$ . With (14), the pmf of  $A$  conditioned on the channel input bit  $X$  is

$$P_{A|X}(a_i|x) = \sum_{\mathbf{r} \in \mathcal{R}^{d_c-1}, \Phi_c(\mathbf{r})=a_i} P_{\mathbf{R}|X}(\mathbf{r}|x), \quad (17)$$

where  $1 \leq i \leq |\mathcal{A}|$ , and  $P_{\mathbf{R}|X}(\mathbf{r}|x)$  is given by (4).

3) *Design principle of  $\Gamma_c$* : Based on  $\mathcal{A}$  and  $P_{A|X}$ , we adopt the general DP method proposed in [21] to find an optimal SDQ

$$\Lambda_c = \{\lambda_0 = 0, \lambda_1, \dots, \lambda_{|\mathcal{S}|-1}, \lambda_{|\mathcal{S}|} = |\mathcal{A}|\} : \mathcal{A} \rightarrow \mathcal{S} \quad (18)$$

to maximize  $I(X; S)$  among all SDQs. Here  $\lambda_1, \lambda_2, \dots, \lambda_{|\mathcal{S}|-1}$  are corresponding to the indices of  $|\mathcal{S}| - 1$  elements in  $\mathcal{A}$ . Based on  $\Lambda_c$ , instead of using (6), we can compute  $P_{S|X}$  for the C2V message  $S$  in a simpler way given by

$$P_{S|X}(s|x) = \sum_{i=\lambda_s+1}^{\lambda_{s+1}} P_{A|X}(a_i|x). \quad (19)$$

Since the indices in  $\Lambda_c$  cannot be directly applied to decoding, we convert the index  $\lambda_i \in \Lambda_c$  ( $1 \leq i \leq |\mathcal{S}| - 1$ ) to the  $\lambda_i$ -th element  $a_{\lambda_i} \in \mathcal{A}$ , which leads to the threshold set (TS)  $\Gamma_c$  given by

$$\Gamma_c = \{\gamma_i = a_{\lambda_i} : 1 \leq i \leq |\mathcal{S}| - 1\}. \quad (20)$$

At this point, the UF  $Q_c : \mathcal{R}^{d_c-1} \rightarrow \mathcal{S}$  is fully determined by  $\phi_c$ ,  $\Phi_c$ , and  $\Gamma_c$  in the following way as

$$Q_c(\mathbf{r}) = \begin{cases} 0 & \Phi_c(\mathbf{r}) \succeq \gamma_1, \\ i & \gamma_i \succ \Phi_c(\mathbf{r}) \succeq \gamma_{i+1}, 1 \leq i \leq |\mathcal{S}| - 2, \\ |\mathcal{S}| - 1 & \gamma_{|\mathcal{S}|-1} \succ \Phi_c(\mathbf{r}), \end{cases} \quad (21)$$

where  $\succeq$  is a binary relation on  $\mathbb{R}$  defined by

$$\alpha \succeq \beta \iff \alpha \succ \beta \text{ or } \alpha = \beta, \text{ for } \alpha, \beta \in \mathbb{R}.$$

Note that the storage complexity of  $Q_c$  given by (21) is  $O(|\mathcal{R}| + |\mathcal{S}|)$  ( $O(|\mathcal{R}|)$  for storing  $\phi_c$  and  $O(|\mathcal{S}|)$  for storing  $\Gamma_c$ ), which is negligible since each element of  $\phi_c$  and  $\Gamma_c$  is a small integer in practice. On the other hand, implementing the CN update shown by Fig. 5 for *one* outgoing message has complexity  $O(d_c + \lceil \log_2(|\mathcal{S}|) \rceil)$ . In particular, computing  $\Phi_c(\mathbf{r})$  has complexity  $O(d_c)$  (binary operations mainly including additions), which allows a binary tree-like parallel implementation; meanwhile, mapping  $\Phi_c(\mathbf{r})$  to  $\mathcal{S}$  based on  $\Gamma_c$  has complexity  $O(\lceil \log_2(|\mathcal{S}|) \rceil)$  (binary comparison operations). Note that the simple implementation for mapping  $\Phi_c(\mathbf{r})$  to  $\mathcal{S}$  indeed benefits from the use of SDQ rather than the optimal DQ. Because if an optimal DQ is used to map  $\Phi_c(\mathbf{r}) \in \mathcal{A}$  to  $\mathcal{S}$  in (18), it requires an additional table of size  $|\mathcal{A}|$  to store this optimal DQ. This is the essential reason why we choose SDQs in the quantization step.

## B. VN Update for MIM-QBP Decoding

As shown by Fig. 6, the VN update for MIM-QBP decoding consists of the following three steps (reconstruction, calculation, and quantization): First, we use RF  $\phi_v$  (resp.  $\phi_{ch}$ ) to map each C2V (resp. channel) message symbol to a number of larger bit width which is called C2V (channel-to-variable) computational message; second, we use a function  $\Phi_v$  to combine all computational messages together as defined by (25) to form the V2C computational message; third, we use an SDQ  $\Gamma_v$  to quantize the V2C computational message into the V2C message symbol. In this way, the UF  $Q_v$  at the VN is fully determined by  $\phi_v, \phi_{ch}, \Phi_v$ , and  $\Gamma_v$ . In the rest of this subsection, we show the principles of designing  $\phi_v, \phi_{ch}, \Phi_v$ , and  $\Gamma_v$  so as to obtain a  $Q_v$  that can maximize  $I(X; R)$ .

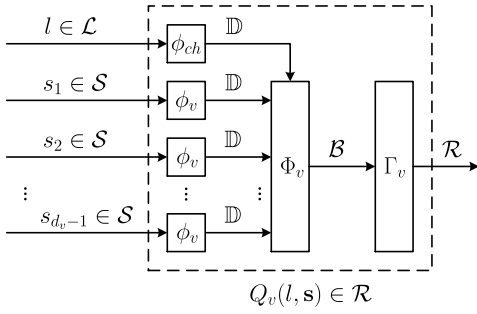


Fig. 6. Variable node update for mutual information-maximizing quantized belief propagation (MIM-QBP) decoding. The part enclosed by the dash square corresponds to the update operation in the VN of Fig. 2(b).

1) *Design principle of  $\phi_v$  and  $\phi_{ch}$* : We use an RF

$$\phi_v : \mathcal{S} \rightarrow \mathbb{D} \quad (22)$$

to map each C2V message realization  $s \in \mathcal{S}$  to  $\phi_v(s) \in \mathbb{D}$ , and use another RF

$$\phi_{ch} : \mathcal{L} \rightarrow \mathbb{D} \quad (23)$$

to map the channel output message realization  $l \in \mathcal{L}$  to  $\phi_{ch}(l) \in \mathbb{D}$ . For  $s \in \mathcal{S}$ , let

$$LLR(s) = \log(P_{X|S}(0|s)/P_{X|S}(1|s)).$$

For  $l \in \mathcal{L}$ , let

$$LLR(l) = \log(P_{X|L}(0|l)/P_{X|L}(1|l)).$$

A good choice for  $\phi_v(s)$  and  $\phi_{ch}(l)$  based on empirical observation is

$$\begin{cases} \phi_v(s) \propto LLR(s), \\ \phi_{ch}(l) \propto LLR(l). \end{cases} \quad (24)$$

Based on (24), we associate  $\phi_v(s)$  and  $\phi_{ch}(l)$  to the channel input bit  $X$  in the following way:  $X$  is more likely to be 0 (resp. 1) for larger (resp. smaller)  $\phi_v(s)$  and  $\phi_{ch}(l)$ .

2) *Design principle of  $\Phi_v$* : For each incoming message realization  $(l, \mathbf{s}) \in \mathcal{L} \times \mathcal{S}^{d_v-1}$ , we combine the corresponding incoming computational messages to form the V2C computational message by

$$\Phi_v(l, \mathbf{s}) = \phi_{ch}(l) + \sum_{i=1}^{\dim(\mathbf{s})} \phi_v(s_i). \quad (25)$$

The channel input bit  $X$  is more likely to be 0 (resp. 1) for smaller (resp. larger)  $\Phi_v(l, \mathbf{s})$ . The calculation step by (25) results in a set of distinct values of  $\Phi_v(l, \mathbf{s}), \forall (l, \mathbf{s}) \in \mathcal{L} \times \mathcal{S}^{d_v-1}$ , which we denote by

$$\mathcal{B} = \{b_1, b_2, \dots, b_{|\mathcal{B}|}\}. \quad (26)$$

The elements in  $\mathcal{B}$  are labelled to satisfy

$$b_1 > b_2 > \dots > b_{|\mathcal{B}|}. \quad (27)$$

Assuming  $\Phi_v(l, \mathbf{s}) = b_i$ , we know from (27) that  $X$  is more likely to be 0 (resp. 1) for smaller (resp. larger)  $i$ . Thus, the

listing order of (27) has a similar feature as the listing order of (2). Let  $B$  be a random variable taking values from  $\mathcal{B}$ . With (25), the pmf of  $B$  conditioned on the channel input bit  $X$  is

$$P_{B|X}(b_i|x) = \sum_{(l, \mathbf{s}) \in \mathcal{L} \times \mathcal{S}^{d_v-1}, \Phi_v(l, \mathbf{s})=b_i} P_{L, \mathbf{S}|X}(l, \mathbf{s}|x), \quad (28)$$

where  $1 \leq i \leq |\mathcal{B}|$  and  $P_{L, \mathbf{S}|X}(l, \mathbf{s}|x)$  is given by (8).

3) *Design principle of  $\Gamma_v$* : Based on  $\mathcal{B}$  and  $P_{B|X}$ , we apply the general DP method in [21] to find an optimal SDQ

$$\Lambda_v = \{\lambda_0 = 0, \lambda_1, \dots, \lambda_{|\mathcal{R}|-1}, \lambda_{|\mathcal{R}|} = |\mathcal{B}|\} : \mathcal{B} \rightarrow \mathcal{R} \quad (29)$$

to maximize  $I(X; R)$  among all SDQs. Here  $\lambda_1, \lambda_2, \dots, \lambda_{|\mathcal{R}|-1}$  are corresponding to the indices of  $|\mathcal{R}| - 1$  elements in  $\mathcal{B}$ . Based on  $\Lambda_v$ , instead of using (9), we can compute  $P_{R|X}$  for the outgoing message  $R$  in a simpler way given by

$$P_{R|X}(r|x) = \sum_{i=\lambda_r+1}^{\lambda_{r+1}} P_{B|X}(b_i|x). \quad (30)$$

Since the indices in  $\Lambda_v$  cannot be directly applied to decoding, we convert the index  $\lambda_i \in \Lambda_v$  ( $1 \leq i \leq |\mathcal{R}| - 1$ ) to the  $\lambda_i$ -th element  $b_{\lambda_i} \in \mathcal{B}$ , which leads to the threshold set (TS)  $\Gamma_v$  given by

$$\Gamma_v = \{\gamma_i = b_{\lambda_i} : 1 \leq i \leq |\mathcal{R}| - 1\}. \quad (31)$$

At this point, the UF  $Q_v : \mathcal{L} \times \mathcal{S}^{d_v-1} \rightarrow \mathcal{R}$  is fully determined by  $\phi_v, \phi_{ch}, \Phi_v$ , and  $\Gamma_v$  in the following way as

$$Q_v(l, \mathbf{s}) = \begin{cases} 0 & \Phi_v(l, \mathbf{s}) \geq \gamma_1, \\ i & \gamma_i > \Phi_v(l, \mathbf{s}) \geq \gamma_{i+1}, 1 \leq i \leq |\mathcal{R}| - 2, \\ |\mathcal{R}| - 1 & \Phi_v(l, \mathbf{s}) < \gamma_{|\mathcal{R}|-1}. \end{cases} \quad (32)$$

Note that the storage complexity of  $Q_v$  given by (32) is  $O(|\mathcal{S}| + |\mathcal{L}| + |\mathcal{R}|)$  ( $O(|\mathcal{S}|)$  for storing  $\phi_v$ ,  $O(|\mathcal{L}|)$  for storing  $\phi_{ch}$ , and  $O(|\mathcal{R}|)$  for storing  $\Gamma_v$ ), which is negligible since each element of  $\phi_v$ ,  $\phi_{ch}$ , and  $\Gamma_v$  is a small integer in practice. On the other hand, implementing the VN update shown by Fig. 6 for *one* outgoing message has complexity  $O(d_v + \lceil \log_2(|\mathcal{R}|) \rceil)$ . In particular, computing  $\Phi_v(l, \mathbf{s})$  has complexity  $O(d_v)$ , which allows a binary tree-like parallel implementation; meanwhile, mapping  $\Phi_v(l, \mathbf{s})$  to  $R$  based on  $\Gamma_v$  has complexity  $O(\lceil \log_2(|\mathcal{R}|) \rceil)$ . The simple implementation for mapping  $\Phi_v(l, \mathbf{s})$  to  $R$  also benefits from the use of SDQ rather than the optimal DQ. Because if an optimal DQ is used instead, it in general requires an additional table of size  $|\mathcal{B}|$  to store this optimal DQ.

### C. Remarks

For each decoding iteration, the design of  $Q_e : \mathcal{L} \times \mathcal{S}^{d_v} \rightarrow \mathcal{X}$  for the MIM-QBP decoding is similar to that of  $Q_v$  introduced in Section III-B. In particular, the same RFs  $\phi_v$  and  $\phi_{ch}$  can be used for the design of  $Q_e$  and  $Q_v$  for a given decoding iteration. We thus ignore the details.

Assume  $|\mathcal{L}|, |\mathcal{R}|, |\mathcal{S}|, I_{\max}$ , and  $\sigma_d$  are given. According to the design framework proposed in this section, it is clear that

the calculation functions  $\Phi_c$  and  $\Phi_v$  are fixed, and the TSs  $\Gamma_c$  and  $\Gamma_v$  are fully determined after choosing RFs  $\phi_c$ ,  $\phi_v$ , and  $\phi_{ch}$ . This results in a great convenience for designing an MIM-QBP decoder, as we only need to find good and even optimal RFs. Furthermore, we propose an efficient design for RFs in the next section.

#### IV. AN EFFICIENT DESIGN OF RECONSTRUCTION FUNCTIONS FOR MIM-QBP DECODER

We illustrated the general framework of the MIM-QBP decoding in Section III. The resulting MIM-QBP decoder works similarly to the quantized BP decoders in [6]–[8]. In fact, we borrow the terms “reconstruction function”, “computational domain”, “unreliability”, and “threshold set” from [6]–[8]. However, the works of [6]–[8] require manual optimization to design the decoder parameters. On the contrary, we propose an efficient way to systematically design practical MIM-QBP decoders in this section under the general framework of Section III. More specifically, we use DE to track the message pmfs, which are given by (17) and (19) for the CN update, and (28) and (30) for the VN update. Based on the evolved message pmfs at each iteration, we design the RFs according to the principles discussed in Section III. We further determine the TSs by the general DP method [21] to obtain the UFs of the MIM-QBP decoder, which aims to maximize  $I(X; S)$  for the CN update and  $I(X; R)$  for the VN update, respectively. The detailed design of the UFs is illustrated as follows.

##### A. Design of $Q_c$ at CN

The design of  $Q_c$  for the CN update consists of designing the RF  $\phi_c$ , the computation of  $\mathcal{A}$  and  $P_{A|X}$ , and determining the TS  $\Gamma_c$ , which corresponds to the three subsections under Section III-A, respectively.

1) *Design of  $\phi_c$* : We first derive the closed-form of the optimal RF  $\phi_c^*$  by setting  $\mathbb{D} = \mathbb{R}$ . Let  $g(r) = P_{X|R}(0|r) - P_{X|R}(1|r)$  for  $r \in \mathcal{R}$  and  $g(\mathbf{r}) = P_{X|\mathbf{R}}(0|\mathbf{r}) - P_{X|\mathbf{R}}(1|\mathbf{r})$  for  $\mathbf{r} \in \mathcal{R}^{d_c-1}$ . Note that  $P_{X|R}$  can be easily derived from  $P_{R|X}$  by Bayes rule with  $P_X(0) = P_X(1) = 1/2$ . For  $r \in \mathcal{R}$ , let

$$\phi_c^*(r) = \begin{cases} \text{sgn}(g(r))\epsilon & |g(r)| = 1, \\ -\text{sgn}(g(r))\log(|g(r)|) & \text{otherwise,} \end{cases} \quad (33)$$

where  $\epsilon$  satisfies

$$0 < \epsilon d_c < \min \{ |\log(|g(\mathbf{r})|) - \log(|g(\mathbf{r}')|)| : \mathbf{r}, \mathbf{r}' \in \mathcal{R}^{d_c-1}, g(\mathbf{r}) \neq g(\mathbf{r}'), \text{sgn}(g(\mathbf{r})) = \text{sgn}(g(\mathbf{r}')) \neq 0 \}. \quad (34)$$

Here  $\epsilon$  is a small number close to 0, which ensures the condition of (13) to be valid for the case of  $\phi_c = \phi_c^*$ . Meanwhile,  $\epsilon$  is necessary for the following theorem.

**Theorem 1:** Consider the computational domain  $\mathbb{D} = \mathbb{R}$  and let  $\phi_c = \phi_c^*$ .  $Q_c$  defined by (21) can maximize  $I(X; S)$  among all quantizers from  $\mathcal{R}^{d_c-1}$  to  $\mathcal{S}$ .

*Proof:* See Appendix A. ■

Theorem 1 indicates that  $\phi_c^*$  is an optimal choice for  $\phi_c$  in terms of maximizing  $I(X; S)$ . Compared to the function

$f(\theta) = \log((e^\theta + 1)/(e^\theta - 1))$  used in [1] and [4] for the CN update,  $\phi_c^*$  is closely related to  $f(\theta)$  in the sense that we have  $f(|LLR(r)|) = -\log(|g(r)|)$  and  $\text{sgn}(LLR(r)) = \text{sgn}(g(r))$  for  $r \in \mathcal{R}$ . This indicates a close connection between the CN update of the BP decoding and that of the MIM-QBP decoding by using the RF  $\phi_c = \phi_c^*$ .

**Corollary 1:** Consider the computational domain  $\mathbb{D} = \mathbb{R}$  and  $\phi_c = \eta\phi_c^*$ , where  $\eta$  is an arbitrary positive real number.  $Q_c$  defined by (21) can maximize  $I(X; S)$  among all quantizers from  $\mathcal{R}^{d_c-1}$  to  $\mathcal{S}$ .

*Proof:* Corollary 1 can be proved similarly to the proof of Theorem 1. ■

Corollary 1 indicates that for  $\mathbb{D} = \mathbb{R}$ , the scaled version of  $\phi_c^*$  is also optimal for  $Q_c$  in the sense of maximizing  $I(X; S)$ . This provides a near-optimal solution for designing  $\phi_c$  by scaling  $\phi_c^*$  for  $\mathbb{D} = \mathbb{Z}$ . In the following, we consider  $\mathbb{D} = \mathbb{Z}$ . Denote the maximum allowed absolute value of  $\phi_c$  by  $|\phi_c|_{\max}$ . Suppose that there are at most  $q_c$  bits allowed for computing the additions by  $\Phi_c$ , where one bit is needed for representing the sign of each outgoing message. We have

$$|\phi_c|_{\max} = \lfloor (2^{q_c-1} - 1)/d_c \rfloor$$

such that  $\sum_{i=1}^{d_c} \phi_c(r_i)$  does not overflow. Let

$$|\phi_c^*|_{\max} = \max\{|\phi_c^*(r)| : r \in \mathcal{R}, g(r) \neq 0\},$$

where  $|\phi_c^*|_{\max} > 0$  holds for a general case. Inspired by Corollary 1, we scale  $\phi_c^*$  approximately by a factor around  $\eta_c = |\phi_c|_{\max}/|\phi_c^*|_{\max}$  to obtain  $\phi_c : \mathcal{R} \rightarrow \mathbb{Z}$  given by

$$\phi_c(r) = \begin{cases} \text{sgn}(g(r)) \max\{1, \text{round}(\eta_c |\phi_c^*(r)|)\} & g(r) \neq 0, \\ |\phi_c|_{\max} & g(r) = 0, \end{cases} \quad (35)$$

where  $\text{round}()$  returns the closest integer of a floating number. In this case, we have  $|\phi_c(r)| \leq |\phi_c|_{\max}, \forall r \in \mathcal{R}$ . Note that for  $g(r) \neq 0$ , we make  $|\phi_c(r)| \geq 1$  to ensure  $\text{sgn}(\phi_c(r)) = \text{sgn}(g(r))$ . In particular, for  $|g(r)| = 1$ , we have  $|\phi_c(r)| = 1$  since  $\epsilon$  is close to 0. Moreover, for  $g(r) = 0$ ,  $r$  has the most unreliability since  $P_{X|R}(0|r) = P_{X|R}(1|r) = 1/2$ . In this case, we use  $\phi_c(r) = |\phi_c|_{\max}$  according to the design principle (13).

2) *Computation of  $\mathcal{A}$  and  $P_{A|X}$* : By using the RF  $\phi_c$  given by (35), the function  $\Phi_c$  defined by (14) is capable of mapping  $\mathcal{R}^{d_c-1}$  to  $\mathbb{Z}$  and obtaining the C2V computational messages represented by  $q_c$ -bit integers. Meanwhile, the integer set  $\mathcal{A}$  and the message pmf  $P_{A|X}$  need to be computed for the decoder design in the quantization step. Note that directly adopting the computation in the ways of (15) and (17) can be a prohibitive task when  $|\mathcal{R}|^{d_c-1}$  is large. In the following, we propose a fast method to compute  $\mathcal{A}$  and  $P_{A|X}$ . The essential idea is using DP [22, Section 15.3] to handle the  $d_c - 1$  V2C message pmfs one by one, and carry out the computation with the previous intermediate results and the current V2C message pmf.

Starting from (4), for  $k \geq 1$  and  $\mathbf{R} \in \mathcal{R}^k$ , we have

$$P_{\mathbf{R}|X}(\mathbf{r}|x) = \left(\frac{1}{2}\right)^{\dim(\mathbf{r})-1} \sum_{\mathbf{x}: \oplus \mathbf{x} = x} \prod_{i=1}^{\dim(\mathbf{r})} P_{R_i|X}(r_i|x_i),$$

which denotes the joint distribution of  $k$  V2C messages conditioned on the channel input bit. Denote the set of distinct values of  $\Phi_c(\mathbf{r})$ ,  $\forall \mathbf{r} \in \mathcal{R}^k$  by

$$\mathcal{A}_k = \{a_{k,1}, a_{k,2}, \dots, a_{k,|\mathcal{A}_k|}\}.$$

Let  $A_k$  be a random variable which takes values from  $\mathcal{A}_k$ . Motivated by (5), we define  $\delta_k^+(\cdot)$  and  $\delta_k^-(\cdot)$  as

$$\begin{aligned} \delta_k^\pm(a_{k,i}) &= \sum_{\mathbf{r} \in \mathcal{R}^k, \Phi_c(\mathbf{r}) = a_{k,i}} (P_{\mathbf{R}|X}(\mathbf{r}|0) \pm P_{\mathbf{R}|X}(\mathbf{r}|1)) \\ &= P_{A_k|X}(a_{k,i}|0) \pm P_{A_k|X}(a_{k,i}|1). \end{aligned}$$

Based on  $\Phi_c$  given by (14), for  $\alpha, \beta \in \mathbb{R}$ , we define  $\diamond$  as a binary operator such that

$$\alpha \diamond \beta = \text{sgn}(\alpha) \text{sgn}(\beta) (|\alpha| + |\beta|).$$

Then we have the following Proposition 1.

**Proposition 1:** For  $k = 1$ , we have

$$\begin{aligned} \mathcal{A}_k &= \{\phi_c(r) : r \in \mathcal{R}\}, \text{ and} \\ \delta_k^\pm(a_{k,i}) &= \sum_{r \in \mathcal{R}, \phi_c(r) = a_{k,i}} (P_{R|X}(r|0) \pm P_{R|X}(r|1)). \end{aligned} \quad (36)$$

For  $k > 1$ , we have

$$\begin{aligned} \mathcal{A}_k &= \{\phi_c(r) \diamond a_{k-1,j} : r \in \mathcal{R}, a_{k-1,j} \in \mathcal{A}_{k-1}\}, \text{ and} \\ \delta_k^\pm(a_{k,i}) &= \sum_{\substack{r \in \mathcal{R}, a_{k-1,j} \in \mathcal{A}_{k-1}, \\ \phi_c(r) \diamond a_{k-1,j} = a_{k,i}}} \frac{1}{2} (P_{R|X}(r|0) \pm P_{R|X}(r|1)) \delta_{k-1}^\pm(a_{k-1,j}). \end{aligned} \quad (37)$$

*Proof:* For  $k = 1$ , (36) holds obviously. For  $k > 1$ , we have

$$\begin{aligned} \mathcal{A}_k &= \{\Phi_c(\mathbf{r}) : \mathbf{r} \in \mathcal{R}^k\} \\ &= \{\phi_c(r) \diamond \Phi_c(\mathbf{r}) : r \in \mathcal{R}, \mathbf{r} \in \mathcal{R}^{k-1}\} \\ &= \{\phi_c(r) \diamond a_{k-1,j} : r \in \mathcal{R}, a_{k-1,j} \in \mathcal{A}_{k-1}\}; \end{aligned}$$

meanwhile, we have

$$\begin{aligned} \delta_k^\pm(a_{k,i}) &= \sum_{\mathbf{r} \in \mathcal{R}^k, \Phi_c(\mathbf{r}) = a_{k,i}} (P_{\mathbf{R}|X}(\mathbf{r}|0) \pm P_{\mathbf{R}|X}(\mathbf{r}|1)) \\ &= \sum_{\mathbf{r} \in \mathcal{R}^k, \Phi_c(\mathbf{r}) = a_{k,i}} \left(\frac{1}{2}\right)^{k-1} \prod_{u=1}^k (P_{R|X}(r_u|0) \pm P_{R|X}(r_u|1)) \\ &= \sum_{r_k \in \mathcal{R}} \frac{1}{2} (P_{R|X}(r_k|0) \pm P_{R|X}(r_k|1)) \times \\ &\quad \sum_{\substack{\mathbf{r} \in \mathcal{R}^{k-1}, \\ \phi_c(\mathbf{r}) \diamond \Phi_c(\mathbf{r}) = a_{k,i}}} \left(\frac{1}{2}\right)^{k-2} \prod_{u=1}^{k-1} (P_{R|X}(r_u|0) \pm P_{R|X}(r_u|1)) \\ &= \sum_{r_k \in \mathcal{R}} \frac{1}{2} (P_{R|X}(r_k|0) \pm P_{R|X}(r_k|1)) \times \\ &\quad \sum_{\substack{\mathbf{r} \in \mathcal{R}^{k-1}, \\ \phi_c(\mathbf{r}) \diamond \Phi_c(\mathbf{r}) = a_{k,i}}} (P_{\mathbf{R}|X}(\mathbf{r}|0) \pm P_{\mathbf{R}|X}(\mathbf{r}|1)) \\ &= \sum_{r \in \mathcal{R}} \frac{1}{2} (P_{R|X}(r|0) \pm P_{R|X}(r|1)) \sum_{\substack{a_{k-1,j} \in \mathcal{A}_{k-1}, \\ \phi_c(r) \diamond a_{k-1,j} = a_{k,i}}} \delta_{k-1}^\pm(a_{k-1,j}). \end{aligned}$$

This completes the proof.  $\blacksquare$

Proposition 1 sets up the recursive computation rules, where for  $k > 1$ ,  $\mathcal{A}_{k-1}$  and  $\delta_{k-1}^\pm$  are the previous intermediate computation results, and they are used to compute  $\mathcal{A}_k$  and  $\delta_k^\pm$  together with the  $k$ -th V2C message  $R$  and its pmf  $P_{R|X}$ . According to Proposition 1, we can compute  $\mathcal{A}_1, \delta_1^\pm, \mathcal{A}_2, \delta_2^\pm, \dots, \mathcal{A}_{d_c-1}, \delta_{d_c-1}^\pm$  sequentially, and obtain the message pmf  $P_{A_k|X}$  by

$$\begin{cases} P_{A_k|X}(a_{k,i}|0) = (\delta_k^+(a_{k,i}) + \delta_k^-(a_{k,i}))/2, \\ P_{A_k|X}(a_{k,i}|1) = (\delta_k^+(a_{k,i}) - \delta_k^-(a_{k,i}))/2. \end{cases}$$

Then, the integer set  $\mathcal{A}$  and the message pmf  $P_{A|X}$  are equal to  $\mathcal{A}_{d_c-1}$  and  $P_{A_{d_c-1}|X}$ , respectively. We summarize the corresponding computation by Algorithm 1. Since  $|\mathcal{A}_{k-1}|$  in line 7 of Algorithm 1 is upper-bounded by  $2^{q_c}$ , the complexity of Algorithm 1 is  $O(d_c 2^{q_c} |\mathcal{R}|)$ .

3) *Determining  $\Gamma_c$ :* Based on  $\mathcal{A}$  and  $P_{A|X}$ , we can compute the optimal SDQ  $\Lambda_c$  by (18). Then we can obtain the pmf  $P_{S|X}$  and the TS  $\Gamma_c$  given by (19) and (20), respectively. The UF  $Q_c$  operates as (21) to compute the C2V messages, where we only need to store  $\phi_c$  and  $\Gamma_c$  for the CN update. The computational complexity is  $O(d_c + d_c \lceil \log_2(|\mathcal{S}|) \rceil)$  for one CN per iteration (including integer comparisons and additions with bit width  $q_c$ ).

## B. Design of $Q_v$ at VN

The design of  $Q_v$  for the VN update contains designing the RFs  $\phi_v$  and  $\phi_{ch}$ , the computation of  $\mathcal{B}$  and  $P_{B|X}$ , and determining the TS  $\Gamma_v$ , which corresponds to the three subsections under Section III-B, respectively.

1) *Design of  $\phi_v$  and  $\phi_{ch}$ :* We first derive the closed-form of the optimal RFs  $\phi_v^*$  and  $\phi_{ch}^*$  by setting  $\mathbb{D} = \mathbb{R}$ . For  $s \in \mathcal{S}$

---

**Algorithm 1** Computation of  $\mathcal{A}$  and  $P_{A|X}$ 

---

**Input:**  $P_{R|X}, \phi_c, d_c$ .**Output:**  $\mathcal{A}$  and  $P_{A|X}$ .

```
1: Set  $\mathcal{A}_k = \emptyset$  and  $\delta_k^\pm(\cdot) = 0$  for  $k = 1, 2, \dots, d_c - 1$ .
2: for  $r \in \mathcal{R}$  do
3:    $\mathcal{A}_1 = \mathcal{A}_1 \cup \{\phi_c(r)\}$ . //See (36)
4:    $\delta_1^\pm(\phi_c(r)) += P_{R|X}(r|0) \pm P_{R|X}(r|1)$ .
5: end for
6: for  $k = 2, 3, \dots, d_c - 1$  do
7:   for  $r \in \mathcal{R}, a_{k-1,j} \in \mathcal{A}_{k-1}$  do
8:      $a_{k,i} = \phi_c(r) \diamond a_{k-1,j}$ .
9:      $\mathcal{A}_k = \mathcal{A}_k \cup \{a_{k,i}\}$ . //See (37)
10:     $\delta_k^\pm(a_{k,i}) += \frac{1}{2}(P_{R|X}(r|0) \pm P_{R|X}(r|1))\delta_{k-1}^\pm(a_{k-1,j})$ .
11:   end for
12: end for
13: for  $k = 1, 2, \dots, d_c - 1$  do
14:   for  $a_{k,i} \in \mathcal{A}_k$  do
15:      $P_{A_k|X}(a_{k,i}|0) = (\delta_k^+(a_{k,i}) + \delta_k^-(a_{k,i}))/2$ .
16:      $P_{A_k|X}(a_{k,i}|1) = (\delta_k^+(a_{k,i}) - \delta_k^-(a_{k,i}))/2$ .
17:   end for
18: end for
19:  $\mathcal{A} = \mathcal{A}_{d_c-1}$ .
20:  $P_{A|X} = P_{\mathcal{A}_{d_c-1}|X}$ .
21: return  $\mathcal{A}$  and  $P_{A|X}$ .
```

---

and  $l \in \mathcal{L}$ , let

$$\begin{cases} \phi_v^*(s) = \log(P_{S|X}(s|0)/P_{S|X}(s|1)), \\ \phi_{ch}^*(l) = \log(P_{L|X}(l|0)/P_{L|X}(l|1)). \end{cases} \quad (38)$$

We can easily verify that the condition of (24) holds for  $\phi_v = \phi_v^*$  and  $\phi_{ch} = \phi_{ch}^*$ . Moreover,  $(\phi_v^*, \phi_{ch}^*)$  is proved to be an optimal choice for  $(\phi_c, \phi_{ch})$  in terms of maximizing  $I(X; R)$  by the following theorem.

**Theorem 2:** Consider the computational domain  $\mathbb{D} = \mathbb{R}$ . Let  $\phi_v = \phi_v^*$  and  $\phi_{ch} = \phi_{ch}^*$ .  $Q_v$  defined by (32) can maximize  $I(X; R)$  among all quantizers from  $\mathcal{L} \times \mathcal{S}^{d_v-1}$  to  $\mathcal{R}$ .

*Proof:* See Appendix B.  $\blacksquare$

Note that we have  $\phi_v^*(s) = LLR(s) + \log(P_X(1)/P_X(0))$  and  $\phi_{ch}^*(l) = LLR(l) + \log(P_X(1)/P_X(0))$ . With  $P_X(1) = P_X(0) = 1/2$ ,  $\phi_v^*$  and  $\phi_{ch}^*$  implies a close relation between the VN update of the BP decoding and that of the MIM-QBP decoding by using  $\phi_v = \phi_v^*$  and  $\phi_{ch} = \phi_{ch}^*$ . To realize fixed-point implementation, we further consider the following corollary.

**Corollary 2:** Consider  $\mathbb{D} = \mathbb{R}$ . Let  $\phi_v = \eta\phi_v^*$  and  $\phi_{ch} = \eta\phi_{ch}^*$ , where  $\eta$  is an arbitrary positive real number.  $Q_v$  defined

by (32) can maximize  $I(X; R)$  among all quantizers from  $\mathcal{L} \times \mathcal{S}^{d_v-1}$  to  $\mathcal{R}$ .

*Proof:* Corollary 2 can be proved in a way similar to the proof of Theorem 2.  $\blacksquare$

Corollary 2 indicates that for  $\mathbb{D} = \mathbb{R}$ , the scaled versions of  $\phi_v^*$  and  $\phi_{ch}^*$  are also optimal for  $Q_v$  with respect to maximizing  $I(X; R)$ . This provides a near-optimal solution for designing  $\phi_v$  and  $\phi_{ch}$  by scaling  $\phi_v^*$  and  $\phi_{ch}^*$ , respectively, for  $\mathbb{D} = \mathbb{Z}$ . In the following, we consider  $\mathbb{D} = \mathbb{Z}$ . Denote the maximum allowed absolute value of  $\phi_v(\cdot)$  and  $\phi_{ch}(\cdot)$  by  $|\phi_{v,ch}|_{\max}$ . Suppose that there are at most  $q_v$  bits allowed for computing the additions by  $\Phi_v$ . Then,  $|\phi_{v,ch}|_{\max}$  can be taken as

$$|\phi_{v,ch}|_{\max} = \lfloor (2^{q_v-1} - 1)/(d_v + 1) \rfloor$$

such that  $\phi_{ch}(l) + \sum_{i=1}^{d_v} \phi_v(s_i)$  does not overflow. Let

$$|\phi_{v,ch}^*|_{\max} = \max(\{|\phi_v^*(s)| : s \in \mathcal{S}\} \cup \{|\phi_{ch}^*(l)| : l \in \mathcal{L}\}).$$

Note that  $|\phi_{v,ch}^*|_{\max} > 0$  holds for a general case. Then, inspired by Corollary 2, we respectively scale  $\phi_v^*$  and  $\phi_{ch}^*$  by a factor around  $\eta_v = |\phi_{v,ch}|_{\max}/|\phi_{v,ch}^*|_{\max}$  to obtain  $\phi_v : \mathcal{S} \rightarrow \mathbb{Z}$  and  $\phi_{ch} : \mathcal{L} \rightarrow \mathbb{Z}$  as follows

$$\begin{cases} \phi_v(s) = \text{sgn}(\phi_v^*(s))\text{round}(\eta_v|\phi_v^*(s)|), \\ \phi_{ch}(l) = \text{sgn}(\phi_{ch}^*(l))\text{round}(\eta_v|\phi_{ch}^*(l)|). \end{cases} \quad (39)$$

In this case, we have  $|\phi_v(s)| \leq |\phi_{v,ch}|_{\max}$  and  $|\phi_{ch}(l)| \leq |\phi_{v,ch}|_{\max}$ .

2) *Computation of  $\mathcal{B}$  and  $P_{B|X}$ :* By using the RFs given by (39), the function  $\Phi_v$  defined by (25) is able to map  $\mathcal{L} \times \mathcal{S}^{d_v-1}$  to  $\mathbb{Z}$  and obtain the V2C computational messages represented by  $q_v$ -bit integers. Similar to the case of the CN update, the integer set  $\mathcal{B}$  and the message pmf  $P_{B|X}$  need to be computed accordingly. However, directly computing  $\mathcal{B}$  and  $P_{B|X}$  by (26) and (28) requires large complexity if  $|\mathcal{L}| \times |\mathcal{S}|^{d_v-1}$  is large. In the following, we propose a fast method to compute  $\mathcal{B}$  and  $P_{B|X}$ . Similar to the case of calculating  $\mathcal{A}$  and  $P_{A|X}$ , the essential idea is adopting DP [22, Section 15.3] to handle the  $d_v$  message pmfs (one channel-to-variable message pmf and  $d_v - 1$  C2V message pmfs) one by one, and carry out the computation with the previous intermediate results and the incoming current message pmf.

Beginning with (8), for  $k \geq 0$ ,  $L \in \mathcal{L}$ , and  $\mathbf{S} \in \mathcal{S}^k$ , we have

$$P_{L,\mathbf{S}|X}(l, \mathbf{s}|x) = P_{L|X}(l|x) \prod_{i=1}^{\dim(\mathbf{s})} P_{S|X}(s_i|x),$$

which denotes the joint distribution of incoming message  $(L, \mathbf{S}) \in \mathcal{L} \times \mathcal{S}^k$  conditioned on the channel input bit  $X$  at a VN. Denote the set of distinct values of  $\Phi_v(l, \mathbf{s}), \forall l \in \mathcal{L}, \forall \mathbf{s} \in \mathcal{S}^k$  by

$$\mathcal{B}_k = \{b_{k,1}, b_{k,2}, \dots, b_{k,|\mathcal{B}_k|}\},$$

In particular, for  $k = 0$ , we have

$$P_{L,\mathbf{S}|X}(l, \mathbf{s}|x) = P_{L|X}(l|x), \text{ and } \Phi_v(l, \mathbf{s}) = \phi_{ch}(l).$$

Let  $B_k$  be a random variable which takes values from  $\mathcal{B}_k$ .

Then we have the following Proposition 2.

**Proposition 2:** For  $k = 0$ , we have

$$\mathcal{B}_k = \{\phi_{ch}(l) : l \in \mathcal{L}\}, \text{ and} \\ P_{\mathcal{B}_k|X}(b_{k,i}|x) = \sum_{l \in \mathcal{L}, \phi_{ch}(l)=b_{k,i}} P_{L|X}(l|x). \quad (40)$$

For  $k > 0$ , we have

$$\mathcal{B}_k = \{\phi_v(s) + b_{k-1,j} : s \in \mathcal{S}, b_{k-1,j} \in \mathcal{B}_{k-1}\}, \text{ and} \\ P_{\mathcal{B}_k|X}(b_{k,i}|x) = \sum_{\substack{s \in \mathcal{S}, b_{k-1,j} \in \mathcal{B}_{k-1}, \\ \phi_v(s) + b_{k-1,j} = b_{k,i}}} P_{S|X}(s|x) P_{\mathcal{B}_{k-1}|X}(b_{k-1,j}|x). \quad (41)$$

*Proof:* For  $k = 0$ , (40) holds obviously. For  $k > 0$ , we have

$$\begin{aligned} \mathcal{B}_k &= \{\Phi_v(l, \mathbf{s}) : l \in \mathcal{L}, \mathbf{s} \in \mathcal{S}^k\} \\ &= \{\phi_v(s) + \Phi_v(l, \mathbf{s}) : s \in \mathcal{S}, l \in \mathcal{L}, \mathbf{s} \in \mathcal{S}^{k-1}\} \\ &= \{\phi_v(s) + b_{k-1,j} : s \in \mathcal{S}, b_{k-1,j} \in \mathcal{B}_{k-1}\}; \end{aligned}$$

meanwhile, we have

$$\begin{aligned} &P_{\mathcal{B}_k|X}(b_{k,i}|x) \\ &= \sum_{l \in \mathcal{L}, \mathbf{s} \in \mathcal{S}^k, \Phi_v(l, \mathbf{s})=b_{k,i}} P_{L, \mathbf{S}|X}(l, \mathbf{s}|x) \\ &= \sum_{l \in \mathcal{L}, \mathbf{s} \in \mathcal{S}^k, \Phi_v(l, \mathbf{s})=b_{k,i}} P_{L|X}(l|x) \prod_{i=1}^k P_{S|X}(s_i|x) \\ &= \sum_{s_k \in \mathcal{S}} P_{S|X}(s_k|x) \sum_{\substack{l \in \mathcal{L}, \mathbf{s} \in \mathcal{S}^{k-1}, \\ \phi_v(s_k) + \Phi_v(l, \mathbf{s})=b_{k,i}}} P_{L|X}(l|x) \prod_{i=1}^{k-1} P_{S|X}(s_i|x) \\ &= \sum_{s_k \in \mathcal{S}} P_{S|X}(s_k|x) \sum_{\substack{l \in \mathcal{L}, \mathbf{s} \in \mathcal{S}^{k-1}, \\ \phi_v(s_k) + \Phi_v(l, \mathbf{s})=b_{k,i}}} P_{L, \mathbf{S}|X}(l, \mathbf{s}|x) \\ &= \sum_{s \in \mathcal{S}} P_{S|X}(s|x) \sum_{\substack{b_{k-1,j} \in \mathcal{B}_{k-1}, \\ \phi_v(s) + b_{k-1,j} = b_{k,i}}} P_{\mathcal{B}_{k-1}|X}(b_{k-1,j}|x). \end{aligned}$$

This completes the proof.  $\blacksquare$

Proposition 2 sets up the recursive computation rules, where we use  $\mathcal{B}_{k-1}$  and  $b_{k-1}$  as the previous intermediate computation results for  $k > 0$  to compute  $\mathcal{B}_k$  and  $b_k$  together with the  $k$ -th incoming message  $S$  and its pmf  $P_{S|X}$ . According to Proposition 2, we can compute  $\mathcal{B}_0, P_{\mathcal{B}_0|X}, \mathcal{B}_1, P_{\mathcal{B}_1|X}, \dots, \mathcal{B}_{d_v-1}, P_{\mathcal{B}_{d_v-1}|X}$  sequentially. Then, the integer set  $\mathcal{B}$  and the message pmf  $P_{\mathcal{B}|X}$  are equal to  $\mathcal{B}_{d_v-1}$  and  $P_{\mathcal{B}_{d_v-1}|X}$ , respectively. We summarize the corresponding computation by Algorithm 2. Since  $|\mathcal{B}_{k-1}|$  in line 7 of Algorithm 2 is upper-bounded by  $2^{q_v}$ , the complexity of Algorithm 2 is  $O(d_v 2^{q_v} |\mathcal{S}|)$ .

3) *Determining  $\Gamma_v$ :* Based on  $\mathcal{B}$  and  $P_{\mathcal{B}|X}$ , we can compute the optimal SDQ  $\Lambda_v$  by (29). Then we obtain the pmf  $P_{R|X}$  and the TS  $\Gamma_v$  given by (30) and (31), respectively. The UF  $Q_v$  operates as (32) to compute the messages passed from VN to CN, where we need to store  $\phi_v, \phi_{ch}$ , and  $\Gamma_v$  for the VN update. The computational complexity is  $O(d_v + d_v \lceil \log_2(|\mathcal{R}|) \rceil)$  for one VN per iteration (including integer comparisons and additions with bit width  $q_v$ ).

---

**Algorithm 2** Computation of  $\mathcal{B}$  and  $P_{\mathcal{B}|X}$

---

**Input:**  $\phi_v, \phi_{ch}, P_{S|X}, P_{L|X}, d_v$ .

**Output:**  $\mathcal{B}$  and  $P_{\mathcal{B}|X}$ .

- 1: Set  $\mathcal{B}_k = \emptyset$  and  $P_{\mathcal{B}_k|X}(\cdot|x) = 0$  for  $k = 0, 1, \dots, d_v - 1$  and for  $x = 0, 1$ .
  - 2: **for**  $l \in \mathcal{L}$  **do**
  - 3:    $\mathcal{B}_0 = \mathcal{B}_0 \cup \{\phi_{ch}(l)\}$ . //See (40)
  - 4:    $P_{\mathcal{B}_0|X}(\phi_{ch}(l)|x) += P_{L|X}(l|x)$  for  $x = 0, 1$ .
  - 5: **end for**
  - 6: **for**  $k = 1, 2, \dots, d_v - 1$  **do**
  - 7:   **for**  $s \in \mathcal{S}, b_{k-1,j} \in \mathcal{B}_{k-1}$  **do**
  - 8:      $b_{k,i} = \phi_v(s) + b_{k-1,j}$ .
  - 9:      $\mathcal{B}_k = \mathcal{B}_k \cup \{b_{k,i}\}$ . //See (41)
  - 10:     $P_{\mathcal{B}_k|X}(b_{k,i}|x) += P_{S|X}(s|x) P_{\mathcal{B}_{k-1}|X}(b_{k-1,j}|x)$  for  $x = 0, 1$ .
  - 11:   **end for**
  - 12: **end for**
  - 13:  $P_{\mathcal{B}|X} = P_{\mathcal{B}_{d_v-1}|X}$ .
  - 14: **return**  $\mathcal{B}$  and  $P_{\mathcal{B}|X}$ .
- 

### C. Remarks

As illustrated by Section III-C, the design of  $Q_e$  is quite similar to that of  $Q_v$ . In particular, the same RFs  $\phi_v$  and  $\phi_{ch}$  can be used for the design of  $Q_e$  and  $Q_v$  for a given decoding iteration, and the design of  $Q_e$  has a complexity of  $O(d_v 2^{q_v} |\mathcal{S}| + 2^{2q_v} |\mathcal{X}|)$  (for one decoding iteration). After the design of  $Q_e$ , implementing  $Q_e$  for one VN for one iteration during decoding has complexity  $O(d_v)$ , which is equal to the complexity of addition operations with  $q_v$  bit widths.

After setting desirable maximum allowed bit widths  $q_c$  for the CN update and  $q_v$  for the VN update, we can obtain the near-optimal practical RFs  $\phi_c$  by (35) and  $(\phi_v, \phi_{ch})$  by (39), which are scaled versions of their optimal counterparts  $\phi_c^*, \phi_v^*$ , and  $\phi_{ch}^*$ , respectively. We remark that if  $q_c$  and  $q_v$  are sufficiently large (e.g., infinite precision is allowed),  $\phi_c, \phi_v$ , and  $\phi_{ch}$  coincide with their optimal counterparts, which can make the MIM-QBP decoder always maximize the MI between the outgoing message and the coded bit according to Corollaries 1 and 2. In this case, the MIM-QBP decoder works the same as the MIM-LUT decoder without table decomposition. On the other hand, for practical implementations with low precision, our design of the RFs based on (35) and (39) may not be optimal anymore. This is because the scaling becomes less accurate with the decrease of  $q_c$  and  $q_v$ . However, our design can still achieve good error rate performance according to extensive simulation results. Furthermore, we believe that the only way to obtain the optimal RFs with low precision is to

conduct the exhaustive search for  $\phi_c$ ,  $\phi_v$ , and  $\phi_{ch}$ , which will be tedious and time-consuming.

At this point, it is clear that setting proper  $(|\mathcal{L}|, |\mathcal{R}|, |\mathcal{S}|, I_{\max}, q_c, q_v, \sigma_d)$  is sufficient for our systematic design of the RCQ parameters of an MIM-QBP decoder. Moreover, we can set  $(|\mathcal{L}|, |\mathcal{R}|, |\mathcal{S}|, I_{\max}, q_c, q_v)$  according to practical considerations, e.g., complexity. On the other hand, similar to the MIM-LUT decoder, the performance of the MIM-QBP decoder also depends greatly on the choice of  $\sigma_d$ . We also refer to  $\sigma^*$  given by (11) as the design threshold of the MIM-QBP decoder. Our simulation results show that the MIM-QBP decoder designed at  $\sigma_d = \sigma^*$  can achieve desirable error rate performance across a wide SNR range.

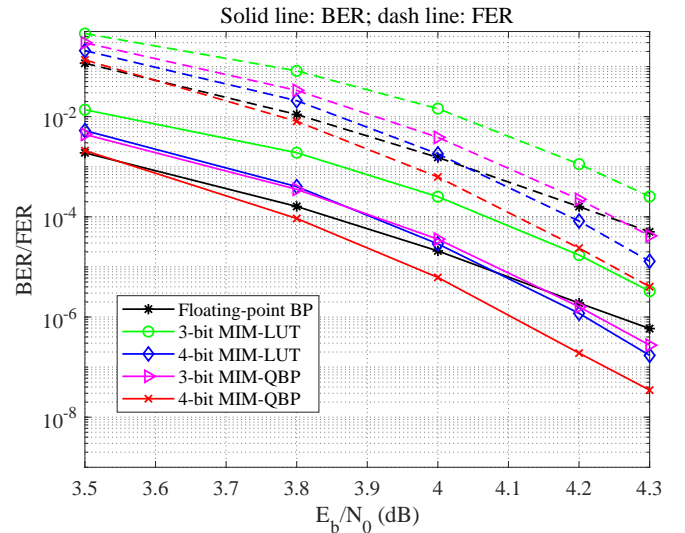
## V. SIMULATION RESULTS

In this section, we evaluate the error rate performance of the proposed MIM-QBP decoders via Monte-Carlo simulations. Assume binary phase-shift keying (BPSK) transmission over the AWGN channel. We design the MIM-QBP decoder by fixing  $|\mathcal{L}| = |\mathcal{R}| = |\mathcal{S}| = 8/16$  (3-/4-bit decoder) for all iterations. We specify  $q_c$  (bit width used for CN update),  $q_v$  (bit width used for VN update), and  $\sigma_d$  (design noise standard deviation) for each specific example. At least 100 frame errors are collected for each simulated SNR.

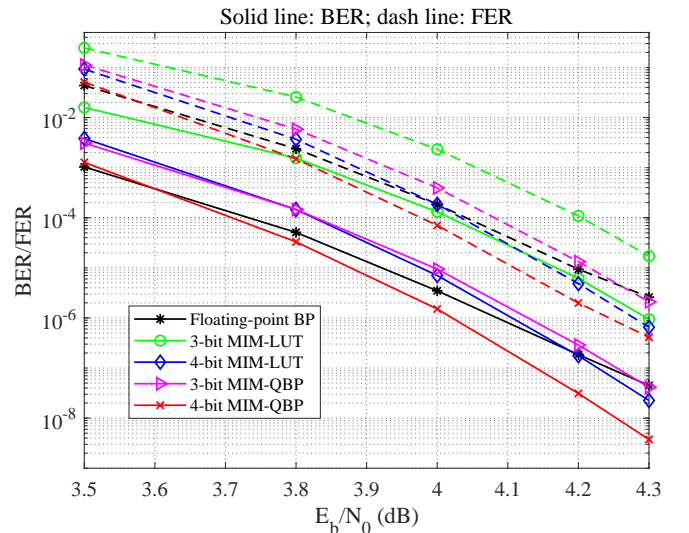
**Example 1:** Consider the regular (6, 32) LDPC code taken from [23]. This code has length 2048 and rate 0.84. We use  $(q_c, q_v) = (10, 8)/(12, 10)$  to design the 3-/4-bit MIM-QBP decoder at  $\sigma_d = 0.5343/0.5417$ , respectively. The bit error rate (BER) and frame error rate (FER) of different decoders are illustrated by Fig. 7. We observe that our proposed 4-bit MIM-QBP decoder outperforms both the 4-bit MIM-LUT decoder [11] and the floating-point BP decoder, with 10/30 iterations, respectively. Moreover, the 3-bit MIM-QBP decoder outperforms the 3-bit MIM-LUT decoder by about 0.15 dB, and even surpasses the floating-point BP decoder at the high SNR region. Note that the degradation of the performance of the floating-point BP decoder is mainly caused by the (8, 8) trapping sets in the code graph [24]. In contrast, our proposed MIM-QBP decoders are designed based on maximizing the mutual information, which may improve the ability to overcome certain trapping sets during the decoding process [9].

**Example 2:** Consider the regular (3, 6) LDPC code with identifier 8000.4000.3.483 taken from [25]. This code has length 8000 and rate 0.5. We use  $(q_c, q_v) = (9, 8)/(10, 10)$  to design the 3-/4-bit MIM-QBP decoder at  $\sigma_d = 0.8479/0.8660$ , respectively. The BER performance of different decoders is presented by Fig. 8. Note that the 3-/4-bit non-uniform QBP decoder [7] requires  $(q_c, q_v) = (9, 8)/(12, 10)$ , respectively. In addition, the design of the corresponding decoders involves much manual optimization, while our proposed MIM-QBP decoders are designed systematically.

From Fig. 8, we observe that the 3-bit MIM-QBP decoder outperforms the 3-bit MIM-LUT decoder [11] by about 0.2 dB, and also performs better than the 3-bit non-uniform QBP decoder [7]. Moreover, the 4-bit MIM-QBP decoder shows almost the same performance as the 4-bit non-uniform decoder



(a) A maximum of 10 iterations.



(b) A maximum of 30 iterations.

Fig. 7. BER and FER simulation results for the (6, 32) code [23] of length 2048 and rate 0.84. We set  $(q_c, q_v) = (10, 8)$  and  $(q_c, q_v) = (12, 10)$  for the 3-bit and 4-bit MIM-QBP decoders, respectively.

by using 2 less bits for the CN update. In addition, the 4-bit MIM-QBP decoder achieves better performance than the 4-bit MIM-LUT decoder [11], and approaches the performance of the floating-point BP decoder within 0.05 dB at the BER of  $10^{-6}$ .

## VI. CONCLUSION

In this paper, we have proposed the MIM-QBP decoding for regular LDPC codes, which follows the RCQ decoding architecture. Notably, we have established the first complete and systematic design framework for the RCQ parameters with respect to that, setting proper  $(|\mathcal{L}|, |\mathcal{R}|, |\mathcal{S}|, I_{\max}, q_c, q_v, \sigma_d)$  is sufficient for the design of the optimal/near-optimal RCQ parameters which are able to maximize  $I(X; S)$  and  $I(X; R)$

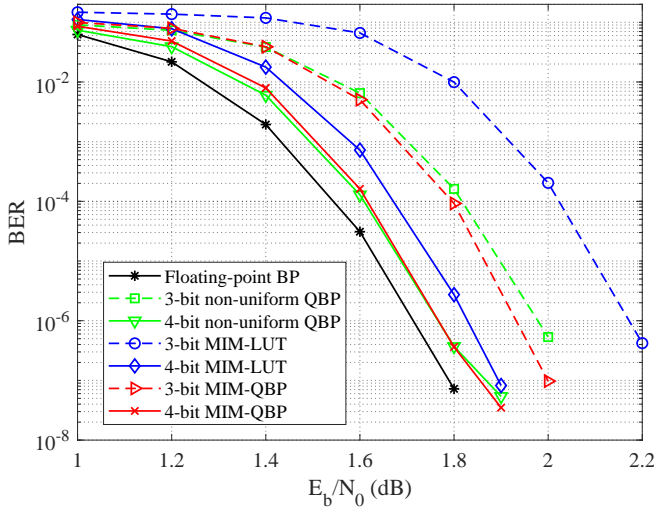


Fig. 8. BER simulation results for the (3, 6) code (with identifier 8000.4000.3.483 in [25]) of length 8000 and rate 0.5. A maximum of 50 iterations is used. We set  $(q_c, q_v) = (9, 8)$  and  $(q_c, q_v) = (10, 10)$  for the 3-bit and 4-bit MIM-QBP decoders, respectively.

for sufficiently large  $q_c$  and  $q_v$ , respectively. In terms of error rate performance, simulation results showed that the MIM-QBP decoder can always considerably outperform the state-of-the-art MIM-LUT decoder [9]–[11]. Moreover, the MIM-QBP decoder has advantages over the floating-point BP decoder when

- the maximum allowed number of decoding iterations is small (generally less than 30), and/or
- the code rate is high, and/or
- the operating SNR is high.

#### APPENDIX A PROOF OF THEOREM 1

Note that  $Q_c$  realizes the quantization from  $\mathcal{R}^{d_c-1}$  to  $\mathcal{S}$  with two steps: First, convert  $\mathcal{R}^{d_c-1}$  to  $\mathcal{A}$  based on  $\Phi_c$  given by (14), and then quantize  $\mathcal{A}$  to  $\mathcal{S}$  based on the quantizer  $\Lambda_c$  given by (18). Therefore, to prove Theorem 1 (i.e.,  $Q_c$  can maximize  $I(X; S)$  among all quantizers from  $\mathcal{R}^{d_c-1}$  to  $\mathcal{S}$ ), it suffices to prove that the following two statements hold:

- The optimal quantizer from  $\mathcal{A}$  to  $\mathcal{S}$  can achieve the same maximum  $I(X; S)$  as the optimal quantizer from  $\mathcal{R}^{d_c-1}$  to  $\mathcal{S}$ .
- $\Lambda_c$  is an optimal quantizer from  $\mathcal{A}$  to  $\mathcal{S}$  which can maximize  $I(X; S)$ .

Let  $\phi_c = \phi_c^*$ . For  $\mathbf{r}, \mathbf{r}' \in \mathcal{R}^{d_c-1}$ , assume  $\Phi_c(\mathbf{r}) = a_i \in \mathcal{A}$  and  $\Phi_c(\mathbf{r}') = a_{i'} \in \mathcal{A}$ , where  $\Phi_c$  and  $\mathcal{A}$  are given by (14) and (15), respectively. We first prove

$$\frac{P_{\mathbf{R}|X}(\mathbf{r}|0)}{P_{\mathbf{R}|X}(\mathbf{r}|1)} > \frac{P_{\mathbf{R}|X}(\mathbf{r}'|0)}{P_{\mathbf{R}|X}(\mathbf{r}'|1)} \Rightarrow i < i', \quad (42)$$

which is sufficient for proving the above two statements.

*Proof of (42):* We start the proof of (42) by showing some properties of  $\Phi_c$ . For  $\mathbf{r} \in \mathcal{R}^{d_c-1}$ , we have

$$g(\mathbf{r}) = \prod_{i=1}^{\dim(\mathbf{r})} g(r_i)$$

according to (5). Let

$$h(\mathbf{r}) = |\{r_i : 1 \leq i \leq \dim(\mathbf{r}), |g(r_i)| = 1\}|.$$

Then, we have

$$\begin{aligned} |\Phi_c(\mathbf{r})| &= \sum_{i=1}^{\dim(\mathbf{r})} |\phi_c^*(r_i)| \\ &= - \sum_{i=1}^{\dim(\mathbf{r})} \log(|g(r_i)|) + h(\mathbf{r})\epsilon \\ &= - \log \left( \prod_{i=1}^{\dim(\mathbf{r})} |g(r_i)| \right) + h(\mathbf{r})\epsilon \\ &= - \log(|g(\mathbf{r})|) + h(\mathbf{r})\epsilon. \end{aligned} \quad (43)$$

Meanwhile, we have

$$\begin{aligned} \text{sgn}(\Phi_c(\mathbf{r})) &= \prod_{i=1}^{\dim(\mathbf{r})} \text{sgn}(\phi_c(r_i)) \\ &= \prod_{i=1}^{\dim(\mathbf{r})} \text{sgn}(g(r_i)) = \text{sgn}(g(\mathbf{r})). \end{aligned} \quad (44)$$

We continue to prove (42). We have

$$\begin{aligned} \frac{P_{\mathbf{R}|X}(\mathbf{r}|0)/P_{\mathbf{R}|X}(\mathbf{r}|1)} &> \frac{P_{\mathbf{R}|X}(\mathbf{r}'|0)/P_{\mathbf{R}|X}(\mathbf{r}'|1)} \\ \Rightarrow \frac{P_{X|\mathbf{R}}(0|\mathbf{r})/P_{X|\mathbf{R}}(1|\mathbf{r})}{P_{X|\mathbf{R}}(0|\mathbf{r}')/P_{X|\mathbf{R}}(1|\mathbf{r}')} &> \\ \Rightarrow g(\mathbf{r}) &> g(\mathbf{r}') \end{aligned}$$

If  $\text{sgn}(g(\mathbf{r})) \neq \text{sgn}(g(\mathbf{r}'))$ , we have

$$\begin{aligned} \frac{P_{\mathbf{R}|X}(\mathbf{r}|0)/P_{\mathbf{R}|X}(\mathbf{r}|1)} &> \frac{P_{\mathbf{R}|X}(\mathbf{r}'|0)/P_{\mathbf{R}|X}(\mathbf{r}'|1)} \\ \Rightarrow \text{sgn}(g(\mathbf{r})) &> \text{sgn}(g(\mathbf{r}')) \\ \stackrel{(a)}{\Rightarrow} \text{sgn}(\Phi_c(\mathbf{r})) &> \text{sgn}(\Phi_c(\mathbf{r}')) \\ \Rightarrow \Phi_c(\mathbf{r}) &> \Phi_c(\mathbf{r}') \\ \stackrel{(b)}{\Rightarrow} i &< i', \end{aligned}$$

where (a) and (b) are based on (44) and (16). Otherwise, we have  $\text{sgn}(g(\mathbf{r})) = \text{sgn}(g(\mathbf{r}')) \neq 0$ , leading to

$$\begin{aligned} \frac{P_{\mathbf{R}|X}(\mathbf{r}|0)/P_{\mathbf{R}|X}(\mathbf{r}|1)} &> \frac{P_{\mathbf{R}|X}(\mathbf{r}'|0)/P_{\mathbf{R}|X}(\mathbf{r}'|1)} \\ \Rightarrow \text{sgn}(g(\mathbf{r}))|g(\mathbf{r})| &> \text{sgn}(g(\mathbf{r}'))|g(\mathbf{r}')| \\ \Rightarrow -\text{sgn}(g(\mathbf{r})) \log(|g(\mathbf{r})|) &< -\text{sgn}(g(\mathbf{r}')) \log(|g(\mathbf{r}')|) \\ \stackrel{(c)}{\Rightarrow} \text{sgn}(g(\mathbf{r}))(-\log(|g(\mathbf{r})|) + h(\mathbf{r})\epsilon) &< \\ &\quad \text{sgn}(g(\mathbf{r}'))(-\log(|g(\mathbf{r}')|) + h(\mathbf{r}')\epsilon) \\ \stackrel{(d)}{\Rightarrow} \Phi_c(\mathbf{r}) &< \Phi_c(\mathbf{r}') \\ \Rightarrow \Phi_c(\mathbf{r}) &> \Phi_c(\mathbf{r}') \\ \stackrel{(e)}{\Rightarrow} i &< i', \end{aligned}$$

where (c), (d) and (e) are based on (34), (43), and (16), respectively. At this point, the proof of (42) is completed.

We are ready to utilize (42) to prove the aforementioned

two statements.

*Proof of the first statement:* Let  $N = |\mathcal{R}|^{d_c-1}$ . We list the elements of  $\mathcal{R}^{d_c-1}$  as  $\{\mathbf{r}_1, \mathbf{r}_2, \dots, \mathbf{r}_N\}$  such that for any  $1 \leq j < j' \leq N$ , assuming  $\Phi_c(\mathbf{r}_j) = a_i \in \mathcal{A}$  and  $\Phi_c(\mathbf{r}_{j'}) = a_{i'} \in \mathcal{A}$ , it holds that  $i \leq i'$ . Based on (42), we have

$$\frac{P_{\mathbf{R}|X}(\mathbf{r}_1|0)}{P_{\mathbf{R}|X}(\mathbf{r}_1|1)} \geq \frac{P_{\mathbf{R}|X}(\mathbf{r}_2|0)}{P_{\mathbf{R}|X}(\mathbf{r}_2|1)} \geq \dots \geq \frac{P_{\mathbf{R}|X}(\mathbf{r}_N|0)}{P_{\mathbf{R}|X}(\mathbf{r}_N|1)}, \quad (45)$$

and for any  $\Phi_c(\mathbf{r}_j) = \Phi_c(\mathbf{r}_{j'}) = a_i \in \mathcal{A}$ , we have

$$\frac{P_{\mathbf{R}|X}(\mathbf{r}_j|0)}{P_{\mathbf{R}|X}(\mathbf{r}_j|1)} = \frac{P_{\mathbf{R}|X}(\mathbf{r}_{j'}|0)}{P_{\mathbf{R}|X}(\mathbf{r}_{j'}|1)} = \frac{P_{A|X}(a_i|0)}{P_{A|X}(a_i|1)}. \quad (46)$$

The above (46) indicates that some elements in  $\mathcal{R}^{d_c-1}$  with the same LLR value are merged into a single element in  $\mathcal{A}$ . However, the optimal quantizer from  $\mathcal{A}$  to  $\mathcal{S}$  can achieve the same maximum  $I(X; S)$  as the optimal quantizer from  $\mathcal{R}^{d_c-1}$  to  $\mathcal{S}$  [20].

*Proof of the second statement:* On the other hand, with (42) and (45), we have

$$\frac{P_{A|X}(a_1|0)}{P_{A|X}(a_1|1)} \geq \frac{P_{A|X}(a_2|0)}{P_{A|X}(a_2|1)} \geq \dots \geq \frac{P_{A|X}(a_{|\mathcal{A}|}|0)}{P_{A|X}(a_{|\mathcal{A}|}|1)}. \quad (47)$$

As a result, the optimal SDQ  $\Lambda_c : \mathcal{A} \rightarrow \mathcal{S}$  given by (18) can maximize  $I(X; S)$  among all quantizers from  $\mathcal{A}$  to  $\mathcal{S}$ , as explained in Section II-A. The proof of Theorem 1 is completed.

## APPENDIX B PROOF OF THEOREM 2

Note that  $Q_v$  realizes the quantization from  $\mathcal{L} \times \mathcal{S}^{d_v-1}$  to  $\mathcal{R}$  with two steps: First, convert  $\mathcal{L} \times \mathcal{S}^{d_v-1}$  to  $\mathcal{B}$  based on  $\Phi_v$  given by (25), and then quantize  $\mathcal{B}$  to  $\mathcal{R}$  based on  $\Lambda_v$  given by (29). Therefore, to prove Theorem 2 (i.e.,  $Q_v$  can maximize  $I(X; R)$  among all quantizers from  $\mathcal{L} \times \mathcal{S}^{d_v-1}$  to  $\mathcal{R}$ ), it suffices to prove that the following two statements hold:

- The optimal quantizer from  $\mathcal{B}$  to  $\mathcal{R}$  can achieve the same maximum  $I(X; R)$  as the optimal quantizer from  $\mathcal{L} \times \mathcal{S}^{d_v-1}$  to  $\mathcal{R}$ .
- $\Lambda_v$  is an optimal quantizer from  $\mathcal{B}$  to  $\mathcal{R}$  which can maximize  $I(X; R)$ .

Let  $\phi_v = \phi_v^*$  and  $\phi_{ch} = \phi_{ch}^*$ . For  $(l, \mathbf{s}), (l', \mathbf{s}') \in \mathcal{L} \times \mathcal{S}^{d_v-1}$ , assume  $\Phi_v(l, \mathbf{s}) = b_i \in \mathcal{B}$  and  $\Phi_v(l', \mathbf{s}') = b_{i'} \in \mathcal{B}$ , where  $\Phi_c$  and  $\mathcal{A}$  are given by (25) and (26), respectively. We first prove

$$\frac{P_{L, \mathbf{S}|X}(l, \mathbf{s}|0)}{P_{L, \mathbf{S}|X}(l, \mathbf{s}|1)} > \frac{P_{L, \mathbf{S}|X}(l', \mathbf{s}'|0)}{P_{L, \mathbf{S}|X}(l', \mathbf{s}'|1)} \Rightarrow i < i'. \quad (48)$$

which is sufficient for proving the above two statements.

*Proof of (48):* For  $(l, \mathbf{s}) \in \mathcal{L} \times \mathcal{S}^{d_v-1}$ , according to (25), we have

$$\Phi_v(l, \mathbf{s}) = \log \left( \frac{P_{L|X}(l|0)}{P_{L|X}(l|1)} \prod_{i=1}^{\dim(\mathbf{s})} \frac{P_{S|X}(s_i|0)}{P_{S|X}(s_i|1)} \right). \quad (49)$$

Then, we have

$$\begin{aligned} \frac{P_{L, \mathbf{S}|X}(l, \mathbf{s}|0)}{P_{L, \mathbf{S}|X}(l, \mathbf{s}|1)} &> \frac{P_{L, \mathbf{S}|X}(l', \mathbf{s}'|0)}{P_{L, \mathbf{S}|X}(l', \mathbf{s}'|1)} \\ &\stackrel{(f)}{\Rightarrow} \frac{P_{L|X}(l|0)}{P_{L|X}(l|1)} \prod_{i=1}^{\dim(\mathbf{s})} \frac{P_{S|X}(s_i|0)}{P_{S|X}(s_i|1)} > \\ &\quad \frac{P_{L|X}(l'|0)}{P_{L|X}(l'|1)} \prod_{i=1}^{\dim(\mathbf{s}')} \frac{P_{S|X}(s'_i|0)}{P_{S|X}(s'_i|1)} \\ &\stackrel{(g)}{\Rightarrow} \Phi_v(l, \mathbf{s}) > \Phi_v(l', \mathbf{s}') \\ &\stackrel{(h)}{\Rightarrow} i < i', \end{aligned}$$

where (f), (g) and (h) hold because of (8), (49), and (27), respectively. At this point, the proof of (48) is completed.

We are ready to utilize (48) to prove the aforementioned two statements.

*Proof of the first statement:* Let  $N = |\mathcal{L}| \cdot |\mathcal{S}|^{d_v-1}$ . We list the elements of  $\mathcal{L} \times \mathcal{S}^{d_v-1}$  as  $\{\mathbf{y}_1, \mathbf{y}_2, \dots, \mathbf{y}_N\}$  such that for any  $1 \leq j < j' \leq N$ , assuming  $\Phi_v(\mathbf{y}_j) = b_i \in \mathcal{B}$  and  $\Phi_v(\mathbf{y}_{j'}) = b_{i'} \in \mathcal{B}$ , it holds that  $i \leq i'$ . Based on (48), we have

$$\frac{P_{L, \mathbf{S}|X}(\mathbf{y}_1|0)}{P_{L, \mathbf{S}|X}(\mathbf{y}_1|1)} \geq \frac{P_{L, \mathbf{S}|X}(\mathbf{y}_2|0)}{P_{L, \mathbf{S}|X}(\mathbf{y}_2|1)} \geq \dots \geq \frac{P_{L, \mathbf{S}|X}(\mathbf{y}_N|0)}{P_{L, \mathbf{S}|X}(\mathbf{y}_N|1)}, \quad (50)$$

and for any  $\Phi_v(\mathbf{y}_j) = \Phi_v(\mathbf{y}_{j'}) = b_i \in \mathcal{B}$ , we have

$$\frac{P_{L, \mathbf{S}|X}(\mathbf{y}_j|0)}{P_{L, \mathbf{S}|X}(\mathbf{y}_j|1)} = \frac{P_{L, \mathbf{S}|X}(\mathbf{y}_{j'}|0)}{P_{L, \mathbf{S}|X}(\mathbf{y}_{j'}|1)} = \frac{P_{B|X}(b_i|0)}{P_{B|X}(b_i|1)}. \quad (51)$$

The above (51) indicates that some elements in  $\mathcal{L} \times \mathcal{S}^{d_v-1}$  with the same LLR value are merged into a single element in  $\mathcal{B}$ . However, the optimal quantizer from  $\mathcal{B}$  to  $\mathcal{R}$  can achieve the same maximum  $I(X; R)$  as the optimal quantizer from  $\mathcal{L} \times \mathcal{S}^{d_v-1}$  to  $\mathcal{R}$  [20].

*Proof of the second statement:* On the other hand, with (48) and (50), we have

$$\frac{P_{B|X}(b_1|0)}{P_{B|X}(b_1|1)} \geq \frac{P_{B|X}(b_2|0)}{P_{B|X}(b_2|1)} \geq \dots \geq \frac{P_{B|X}(b_{|\mathcal{B}|}|0)}{P_{B|X}(b_{|\mathcal{B}|}|1)}. \quad (52)$$

As a result, the optimal SDQ  $\Lambda_v : \mathcal{B} \rightarrow \mathcal{R}$  given by (29) can maximize  $I(X; R)$  among all quantizers from  $\mathcal{B}$  to  $\mathcal{R}$ , as explained in Section II-A. The proof of Theorem 2 is completed.

## ACKNOWLEDGMENT

This work was supported by National Natural Science Foundation of China (Grant Nos. 62101462 and 62201258), by Natural Science Foundation of Sichuan (Grant No. 2022NS-FSC0952), by Singapore Ministry of Education Academic Research Fund Tier 2 T2EP50221-0036 and MOE2019-T2-2-123.

## REFERENCES

- [1] R. G. Gallager, "Low-density parity-check codes," *IRE Trans. Inf. Theory*, vol. 8, no. 1, pp. 21–28, Jan. 1962.

- [2] P. Chen, K. Cai, and S. Zheng, "Rate-adaptive protograph LDPC codes for multi-level-cell NAND flash memory," *IEEE Commun. Lett.*, vol. 22, no. 6, pp. 1112–1115, Jun. 2018.
- [3] C. A. Aslam, Y. L. Guan, and K. Cai, "Edge-based dynamic scheduling for belief-propagation decoding of LDPC and RS codes," *IEEE Trans. Commun.*, vol. 65, no. 2, pp. 525–535, Feb. 2017.
- [4] J. Chen, A. Dholakia, E. Eleftheriou, M. P. Fossorier, and X.-Y. Hu, "Reduced-complexity decoding of LDPC codes," *IEEE Trans. Commun.*, vol. 53, no. 8, pp. 1288–1299, Aug. 2005.
- [5] Z. Zhang, L. Dolecek, B. Nikolic, V. Anantharam, and M. J. Wainwright, "Design of LDPC decoders for improved low error rate performance: quantization and algorithm choices," *IEEE Trans. Commun.*, vol. 57, no. 11, pp. 3258–3268, Nov. 2009.
- [6] T. J. Richardson and R. L. Urbanke, "The capacity of low-density parity-check codes under message-passing decoding," *IEEE Trans. Inf. Theory*, vol. 47, no. 2, pp. 599–618, Feb. 2001.
- [7] J.-S. Lee and J. Thorpe, "Memory-efficient decoding of LDPC codes," in *Proc. IEEE Int. Symp. Inf. Theory*, Sep. 2005, pp. 459–463.
- [8] J. Thorpe, "Low-complexity approximations to belief propagation for LDPC codes," Oct. 2002. [Online]. Available: <http://www.systems.caltech.edu/~jeremy/research/papers/low-complexity.pdf>
- [9] F. J. C. Romero and B. M. Kurkoski, "LDPC decoding mappings that maximize mutual information," *IEEE J. Sel. Areas Commun.*, vol. 34, no. 9, pp. 2391–2401, Sep. 2016.
- [10] J. Lewandowsky and G. Bauch, "Information-optimum LDPC decoders based on the information bottleneck method," *IEEE Access*, vol. 6, pp. 4054–4071, Jan. 2018.
- [11] M. Meidlinger, G. Matz, and A. Burg, "Design and decoding of irregular LDPC codes based on discrete message passing," *IEEE Trans. Commun.*, vol. 68, no. 3, pp. 1329–1343, Mar. 2020.
- [12] D. J. C. MacKay, "Good error-correcting codes based on very sparse matrices," *IEEE Trans. Inf. Theory*, vol. 45, no. 2, pp. 399–431, Mar. 1999.
- [13] X. He, K. Cai, and Z. Mei, "On mutual information-maximizing quantized belief propagation decoding of LDPC codes," in *Proc. IEEE Global Commun. Conf.*, Dec. 2019, pp. 1–6.
- [14] L. Wang, C. Terrill, M. Stark, Z. Li, S. Chen, C. Hulse, C. Kuo, R. D. Wesel, G. Bauch, and R. Pitchumani, "Reconstruction-computation-quantization (RCQ): A paradigm for low bit width LDPC decoding," *IEEE Trans. Commun.*, vol. 70, no. 4, pp. 2213–2226, Apr. 2022.
- [15] P. Mohr, G. Bauch, F. Yu, and M. Li, "Coarsely quantized layered decoding using the information bottleneck method," in *Proc. IEEE Int. Conf. Commun.*, Jun. 2021, pp. 1–6.
- [16] P. Kang, K. Cai, X. He, and J. Yuan, "Memory efficient mutual information-maximizing quantized min-sum decoding for rate-compatible LDPC codes," *IEEE Commun. Lett.*, vol. 26, no. 4, pp. 733–737, Apr. 2022.
- [17] P. Kang, K. Cai, X. He, S. Li, and J. Yuan, "Generalized mutual information-maximizing quantized decoding of LDPC codes with layered scheduling," *IEEE Trans. Veh. Tech.*, vol. 71, no. 7, pp. 7258–7273, Jul. 2022.
- [18] P. Kang, K. Cai, and X. He, "Design of mutual-information-maximizing quantized shuffled min-sum decoder for rate-compatible quasi-cyclic LDPC codes," *Electronics*, vol. 11, no. 19, Oct. 2022.
- [19] C. Lv, X. He, P. Kang, K. Cai, J. Xing, and X. Tang, "Mutual information-maximizing quantized layered min-sum decoding of QC-LDPC codes," in *Proc. IEEE Global Commun. Conf.*, Dec. 2022, pp. 1–6.
- [20] B. M. Kurkoski and H. Yagi, "Quantization of binary-input discrete memoryless channels," *IEEE Trans. Inf. Theory*, vol. 60, no. 8, pp. 4544–4552, Aug. 2014.
- [21] X. He, K. Cai, W. Song, and Z. Mei, "Dynamic programming for sequential deterministic quantization of discrete memoryless channel," *IEEE Trans. Commun.*, vol. 69, no. 6, pp. 3638–3651, Jun. 2021.
- [22] T. H. Cormen, C. E. Leiserson, R. L. Rivest, and C. Stein, *Introduction to Algorithms: 2nd Edition*. Cambridge, MA, USA: MIT Press, 2001.
- [23] *IEEE standard for information technology—telecommunications and information exchange between systems—local and metropolitan area networks-specific requirements part 3: Carrier sense multiple access with collision detection (CSMA/CD) access method and physical layer specifications*, IEEE Std. 802.3an, Sep. 2006.
- [24] W. Ryan and S. Lin, *Channel codes: classical and modern*. Cambridge University Press, 2009.
- [25] D. J. C. MacKay, "Encyclopedia of sparse graph codes." [Online]. Available: <http://www.inference.phy.cam.ac.uk/mackay/codes/data.html>